2011-01-01

Evidence Of Ancient Rifts Beneath Texas

Keisuke Irie
University of Texas at El Paso, moaiscream1205@gmail.com

EVIDENCE OF ANCIENT RIFTS BENEATH TEXAS

KEISUKE IRIE

Department of Geology Sciences

APPROVED:

Aaron Velasco, Ph.D., Chair

Diane Doser, Ph.D.

Leticia Velázquez, Ph.D.

Benjamin C. Flores, Ph.D.
Interim Dean of the Graduate School

EVIDENCE OF ANCIENT RIFTS BENEATH TEXAS

by

KEISUKE IRIE, B.S.

THESIS

Presented to the Faculty of the Graduate School of

The University of Texas at El Paso

in Partial Fulfillment

of the Requirements

for the Degree of

MASTER OF SCEINCE

Department of Geological Sciences

THE UNIVERSITY OF TEXAS AT EL PASO

December 2011

ACKNOWLEDGEMENT

I would like to thank Dr. Diane I. Doser, Dr. Leticia Velazquez and Dr. Elizabeth Y. Anthony for all of their help and guidance throughout this study. I also want to thank UTEP and Cyber-Share for the funding and support on this study. I want to thank Carlos Montana for all of his assistance with my computer and software problems. I also want to thank my lab mates Ezer Patlan and Lennox Thompson who helped processing data. Lastly, I would like to thank Dr. Aaron A. Velasco, my graduate advisor, for his guidance and supports during last 2 years.

ABSTRACT

Continental rifts are defined as geological features where Earth's lithosphere is pulled away by surface expansion of the Earth. Their physiographic features include linear rift valleys associated with active volcanism. Many rifts fail to split a continent and ancient rifts that failed to split can be found by using seismic waves to image these ancient structures. Using seismic data collected by EarthScope USArray stations in Texas, teleseismic receiver functions was calculated and utilized surface wave dispersion curves to simultaneously invert for the 2D velocity structure beneath each seismic station. EarthScope is a scientific program funded by NSF that provides geophysical data from all around the United States to students and researcher for free. The data for this research came from USArray, the network of 400 transportable seismic stations now stationed in the central US states, including Texas. With the calculated receiver functions, a map was produced to show preliminary 3-D crust/upper mantle boundary structure and the velocity ratio of P and S waves. Based on this in formation, receiver function results allow us locate and analyze ancient rift zones that exist in Texas that are characterized by a shallow crust mantle boundary and high velocity ratio. Finally, with this information on ancient rifts, comparison will be made between the result from this research and the Rio Grande Rift in New Mexico. The goal for this comparison is to determine whether Rio Grande rift is still active or doomed to be another failed rift.

TABLE OF CONTENTS

LIST OF FIGURES

INTRODUCTION

A rift is a geological feature generated by the extension within a plate. If a rift continues to expand, the rift zone becomes a continental or oceanic spreading center. However, not every rift becomes a spreading center. Some rifts become "failed rifts" because they failed to completely break up a plate during the rifting process.

Previous gravity and magnetic surveys have determined that Texas experienced continental rifting and continental subduction/orogenies around 1000-1200Ma (Adams and Keller 1993). In addition to these tectonic activities in the late Precambrian central and west Texas, previous research has also shown that the Texas coastline forms the edge of a rift that separated Yucatan peninsula from Texas during in the late Triassic (Mickus, 2009).

In order to understand the past volcanic and tectonic activities in these areas in more detail, I performed a receiver function survey in the state of Texas using seismic data from the EarthScope's USArray, a network of 400 seismic stations that has been moved across the states west to east between 2004 and 2019. By determining the Moho depth and P wave to S wave seismic velocity ratio (Vp/Vs) from receiver functions, these results provide information on crustal thickness and rock properties of the area. Knowing that rifting processes tend to produce shallow crustal thicknesses, the Moho depth determined by the receiver function survey should indicate the locations of buried rifts. High values of Vp/Vs indicate evidence for partial melting (active rifting) and low values indicate cooler materials with no evidence of present day heating (failed or no rifting). For my research, I created 3D maps based on these receiver function results to analyze and verify past results of gravity and magnetic surveys that identified possible failed rift zones in Texas. This study provides important new seismological constraints on crustal structure in Texas since this is the first time a dense seismic network has operated in the state.

Moreover, the results will be compared with the more extensively studied Rio Grande rift to determine whether this rift in West Texas/New Mexico is currently active or has failed.

TECTONIC SETTING

For the tectonic setting, I will be concentrating on the three major geological provinces found in Texas that will be influencing my receiver function results (Moho thickness and velocity ratio). Therefore, the contents in this part of my thesis will not cover all of tectonic history of Texas.

The continental crust of much of Texas forms a part of the Southern Granite-Rhyolite province that was generated approximately 1.37 GA like many areas of Southern Laurentia (Anthony 2005). Following this event, the Grenville Orogen (approximately 1.1GA) formed the Rodinia continent which covered most of modern day east coast and Gulf coast of the United States. Subsurface and geophysical data show that segments of the Grenville deformation front are found in the Llano uplift in Texas (Thomas 2006).

The Llano uplift was initially created by the collision of two continental plates. Throughout the Grenville orogeny, parts of the Laurentian continent subducted beneath the Southern continent beginning around 1150Ma (Mosher, Levine and Carlson, 2008). As the Laurentian continent collided with the Southern continent, the collision caused jamming of the subduction zone and formed uplifts near the surface. Due to continuing tectonic movement of the Laurentian continent at its subduction zone, the subducting slab of the Laurentian continent was detached from the rest of plate leaving the upper crust of the plate at the surface. This break off in subduction caused upwelling of basaltic magma and melting of the lower crust of the Llano uplift. Therefore, the area deviates from other regions that have experienced continental extension, and the Llano uplift has a slightly thinner continental crust and evidence of magma upwelling (figure 1) (Mosher, Levine and Carlson, 2008).

Following the Grenville orogeny, three major tectonic events occurred in Texas. These events are responsible for the crustal differences between the interior and coastal Texas. First, a rifting event in the Early Cambrian (~530Ma) split the Rodinia continent and formed the Iapetus Ocean (Raye 2011). In Texas, this rifting occurred southeast of the Llano uplift almost parallel to the current Texas Gulf coast. Because of this rifting event, the Grenville Orogen segment in Texas was isolated from other segments of the Grenville Orogen in the eastern United States. Throughout Paleozoic time, a passive continental margin existed between Laurentia and the Iapetus Ocean (Thomas 2006).

A second tectonic event occurred during Pennsylvanian time (~350Ma). During the formation of Pangea, plate collision between the Laurentia and Gondwana continents closed the Iapetus Ocean and formed the Ouachita orogeny (Raye 2011).

The third tectonic event affecting Texas was a rifting event that occurred in the interior of Pangea. The Texas-Gulf of Mexico coastline experienced continental extension after the formation of the Eagle Mills rift basin in Southern Arkansas, and large uplift events occurred in central Texas in late Triassic that caused separation of Texas from the Yucatan peninsula (Mickus, 2009). This continental extension led to ocean floor spreading in late Jurassic (160-145Ma) and formed the Gulf of Mexico. Similar to the Iapetus Ocean opening, the opening of Gulf of Mexico again created passive continental margins along southeastern Texas (Raye 2011).

The major geological provinces in Texas are shown in Figure 2. As described above, the Texas interior is composed of Mesoproterozoic craton formed in 1.3 Ga. The areas near the Gulf coast are composed of transitional crust. Between transitional crust and the Mesoproterozoic craton, the Ouachita Orogen exists as the result of continent collision in Pennsylvanian time. The Gulf of Mexico is composed of Jurassic age oceanic lithosphere related to the ocean floor

spreading in the late Jurassic. Therefore the ages of crusts become younger from northwestern Texas to Southeastern Texas or the Gulf of Mexico (Raye 2011).

In past studies, both seismic and non-seismic data were used to investigate the gradual change of crust from Mesoproterozoic continental to Jurassic oceanic crust in Texas. Magnetic and gravity surveys performed near the Texas coastline show anomaly amplitudes and widths similar to other volcanic rift margins like Namibia (Corner, 2002). Based on a model constructed with various geophysical data including seismic reflection and refraction data, Mickus (2009) concluded that high density and magnetic susceptibility values in southeast Texas resemble a volcanic rifted margin showing a transition from continental lithosphere to Jurassic oceanic lithosphere. A cross section map constructed by Mickus that extends between Llano, Texas and the Gulf of Mexico shows the Moho depth decreases significantly from northwest to southeast direction (Figure 3)

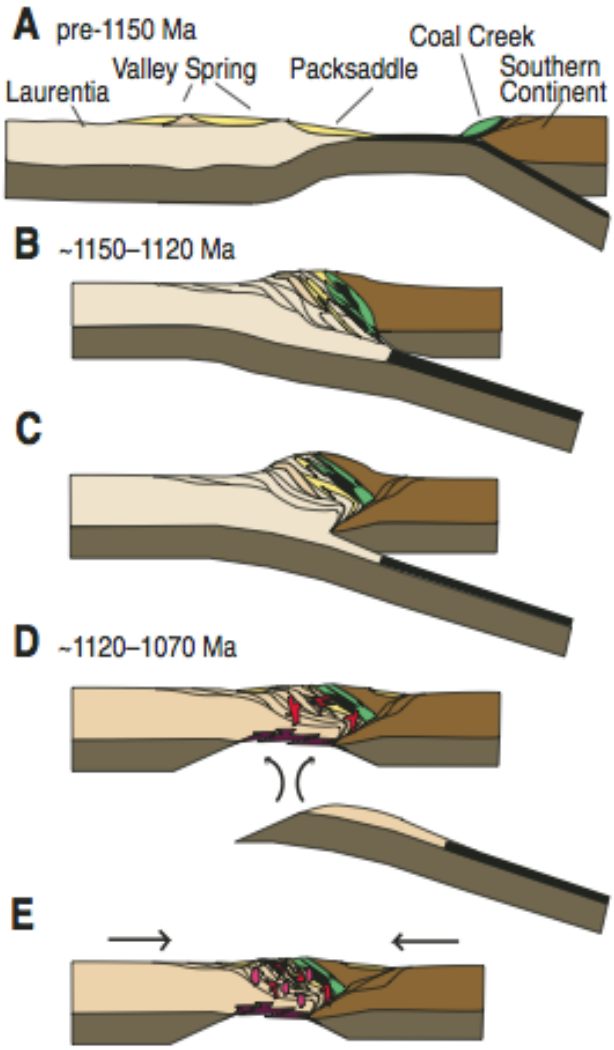

Figure 1: Evolution of Llano uplift from Mosher, Levine and Carlson (2008): This figure illustrates the development of the Grenville orogeny along southern margin of Laurentia. Although the Llano region did not form rifts, because of the detachment of the subducting slab around 1120-1070Ma, the crustal thickness of the Llano uplift is assumed to be thinner than surrounding areas.

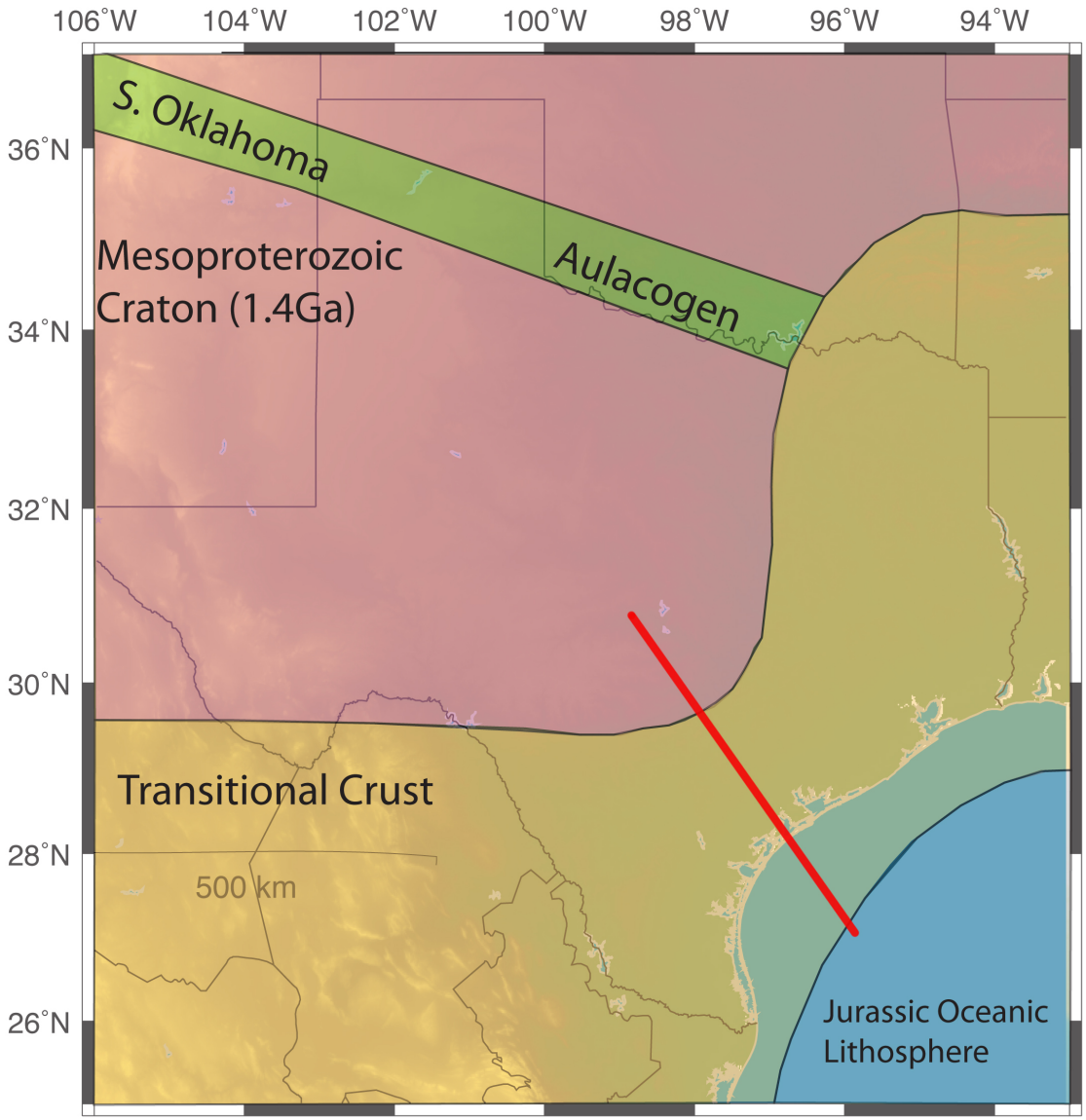

Figure 2: Map of Texas with major geological provinces: The pink area represents Mesoproterozoic craton which lies beneath much of interior Texas The yellow area is transitional crust that formed after continent collision in Pennsylvanian time. The blue Jurassic oceanic lithosphere is generated as an outcome of ocean floor spreading that formed the Gulf of Mexico. A cross section along the red line on this map is illustrated in figure 3. The South Oklahoma Aulacogen splits the Mesoproterozoic craton near the boundary between Oklahoma and Texas. This Aulacogen belt contains dense mafic materials that may affect seismic velocity ratios (Raye 2011).

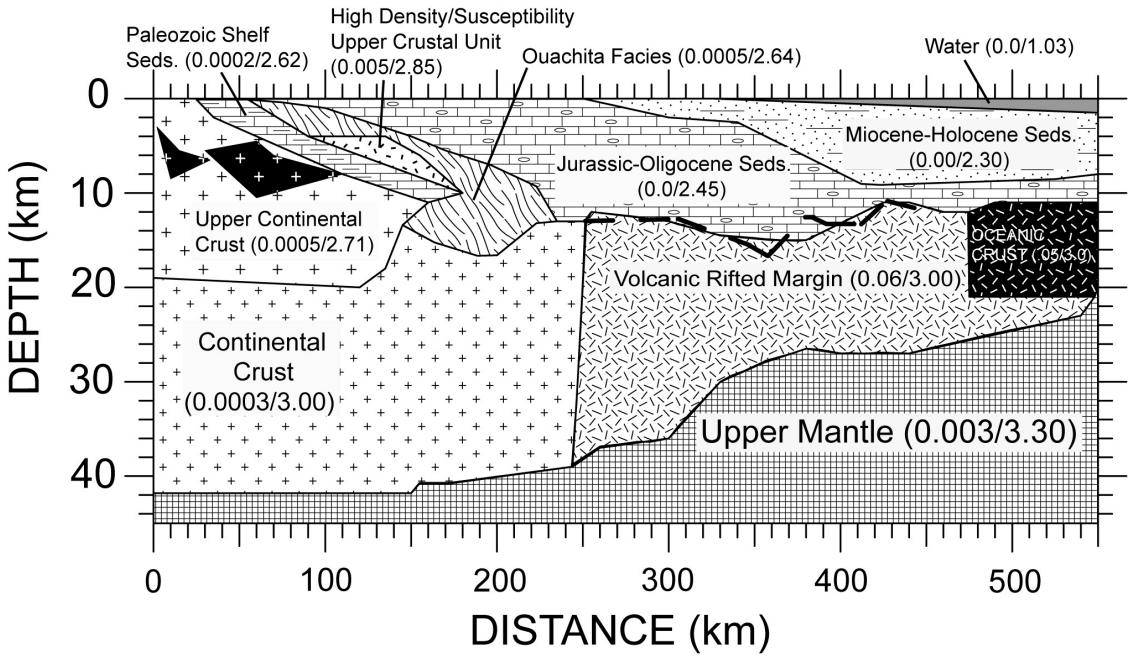

Figure 3: Cross section across the Texas coastal line from Mickus(2009) based on gravity, magnetic, seismic refraction and reflection data. Cross section is taking along the red line shown in Figure 2. The Mesoproterozoic craton (shown in dot pattern) has thickness of over 40km and the crust thins toward the Gulf of Mexico. Numbers in parentheses are magnetic susceptibility (emu) and density (gm/cm^3) of each body.

DATA

EarthScope is a program funded by the National Science Foundation that provides students and researchers geophysical data from regions across the United States. EarthScope consists of deployment of three different types of instrumentation: seismometers, GPS and strainmeters. The USArray is a seismic network consisting of thousands of seismograph stations deployed across the United States. By gathering seismic data from different part of the United States, USArray provides new information to aid regional geophysical studies. In addition to USArray, thousand of GPS instruments have been placed near the North American/Pacific plate boundaries to study plate boundary dynamics, active tectonics and seismic and magmatic processes. There are also 87 strainmeters installed in the United States that monitor strain changes in boreholes and detect very small changes in borehole shape. These three large-scale datasets help us understand Earth structure, evolution of the North American continent and the causes of earthquakes and volcanic eruptions in the United States in great detail.

For this research, I am using the USarray seismic network which consists of three types of seismic stations: Flexible Array, Transportable Array and Reference Network. The Transportable Array is a network of 400 high quality three-component seismographs with 70km station spacing. Unlike other types of stations, the Transportable Array moves station locations eastward every 2 years. In Texas, parts of the Transportable Array were deployed to western Texas in 2008. Between 2009 and 2010, these Transportable Array receivers in western Texas were moved to central and eastern Texas (Figure 3). The Reference Network consists of permanent stations that are separated by 300km spacing across the United States. Because they are permanent stations, they store more events information compared to the Transportable Array.

In Texas, there are 10 Reference Network stations and I collected data from 8 stations that are located in central and eastern Texas.

I requested seismogram data from the Incorporated Research Institutes for Seismology (IRIS) Data Management Center (DMC) for teleseismic events occurring from January of 2008 to September of 2011 for Transportable Array stations and January 2007 to September 2011 for Reference Network stations. Teleseismic events are earthquakes that occurred at distances of 30 to 90 degrees away from a receiver. The reason for using these specific types of seismic events will be explained in the section on receiver functions. These data are requested through a computer program called Standing Order of Data (SOD). When requesting data through SOD, various information has to be specified to obtain seismic data from desired locations with a desired magnitude range. SOD kml codes take maximum/minimum latitudes and longitudes of target areas and extract data from receiver stations that exist within these ranges. In order to reduce amounts of unnecessary data, such as data from Mexico and neighboring states, I collected seismic data from Texas by splitting Texas into 3 areas, west, central and east Texas (figure 4). I requested seismic data for events larger than magnitude 5.5. Due to the teleseismic distance between the source and receivers, magnitudes have to be large enough so that seismic signals received at Texas show strong arrivals and are distinguishable from background noise.

Finally, when requesting data through SOD, I needed to set up a network code and catalog. The network code sets up types of networks used to collect seismic data. In this research the TA network code was used for the Transportable Array stations and the TA, US and IU network codes were used for the Reference Network stations. The catalog is a seismic events database. There are eleven different catalogs and each of them stores data in different formats. In this research I used the PREFFERED catalog and SPYDER catalog. The PREFFERED or

PREF catalog has the most accurate data compared to other catalogs according to IRIS Data Management Center (DMC). SPYDER is the IRIS DMC'S near-real-time data retrieval system that holds the newest seismic data from USArray stations. Although the SPYDER catalog provides data immediately after an event, the data in SPYDER is not quality controlled. To gather seismic data for this research, the PREF catalog was used to collect data from 2007 to 2010 and the SPYDER catalog was used to obtain seismic data from 2011 (IRIS, 2011).

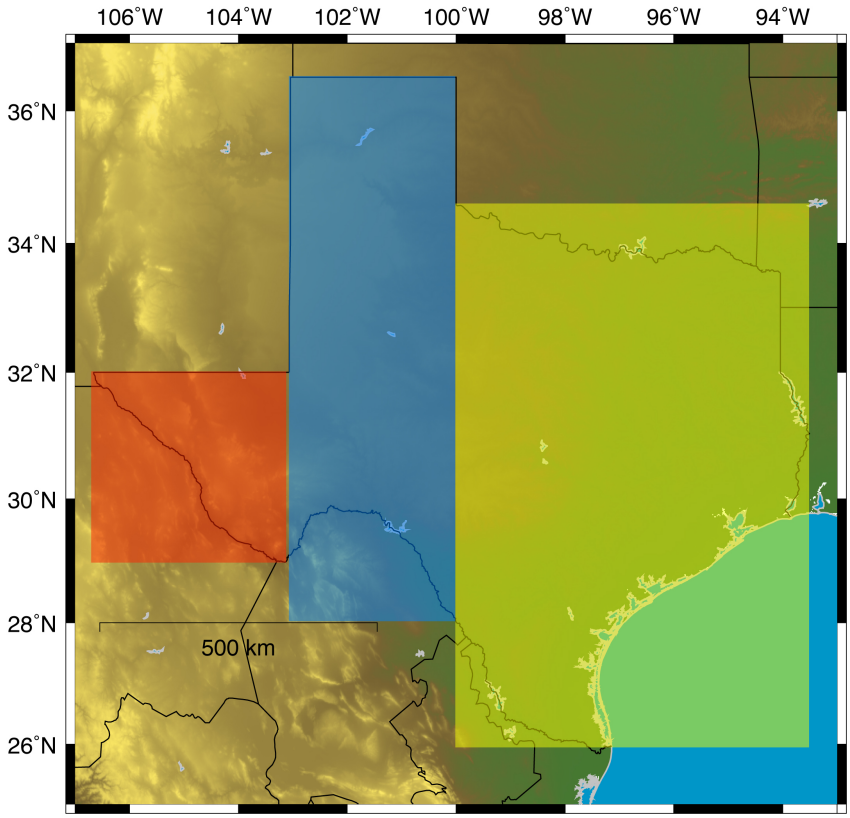

Figure 4: Seismic data collecting method: Seismic data from the Texas Transportable Array and Reference Network stations were collected by selecting 3 rectangular target areas; west Texas (minimum longitude and latitude: -106, 28.95 maximum: -103.065, 32), central Texas (min: -103.06, 28 max: -100, 36.5) and east Texas (min: -100, 26.4 max: -93.8, 34.585). This method minimizes the number of seismic data collected from outside of Texas and reduced the time for collecting seismic data.

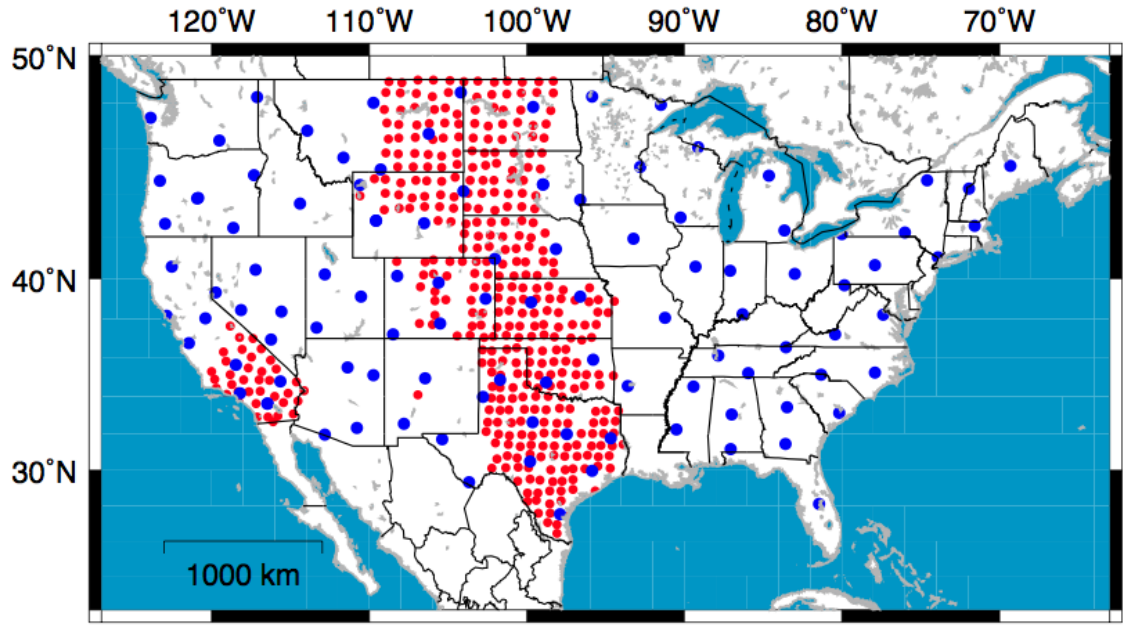

Figure 5: Location of USArray in May 2010: Blue dots are Reference Network stations and red dots are Transportable Array stations. In this thesis I concentrated on Transportable Array and Reference Network stations in Texas.

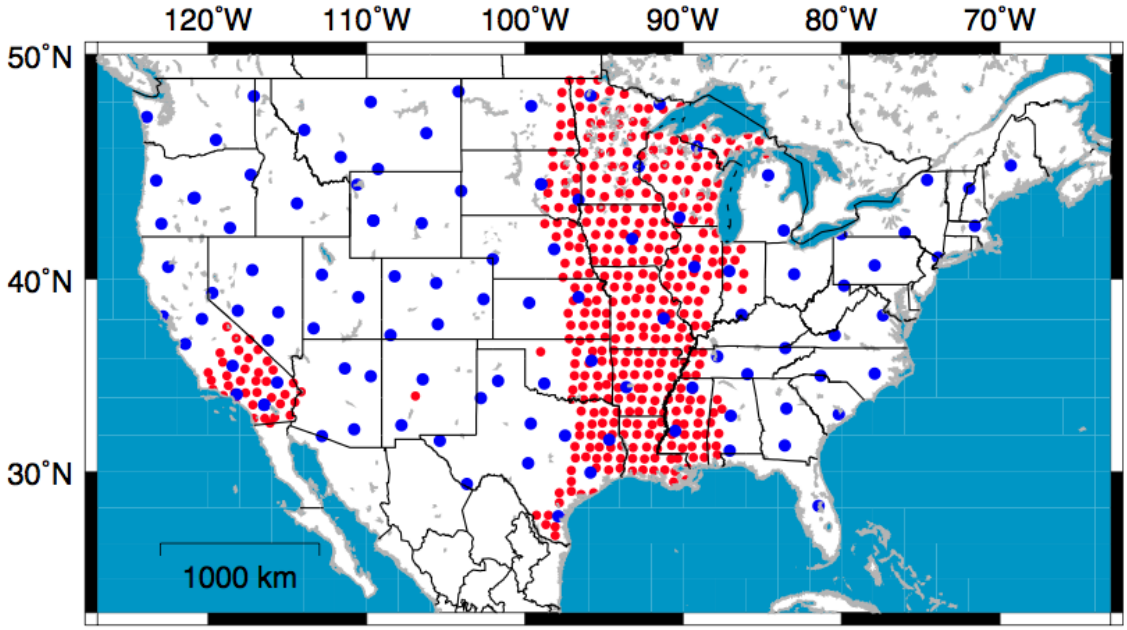

Figure 6: Location of USArray in November 2011: Blue dots are reference network stations and red dots are transportable array stations. Most of the receiver stations in central Texas stopped recording data and moved to different locations in the time period between 2010 and 2011.

METHODS

Receiver Functions

When seismic waves are detected through a three-component seismograph, the wave data obtained from each component can be described as following:

$$D_V(t) = I(t) * S(t) * E_V(t) \quad (1)$$

$$D_R(t) = I(t) * S(t) * E_R(t) \quad (2)$$

$$D_T(t) = I(t) * S(t) * E_T(t) \quad (3)$$

where D_V, D_R, D_T are time domain functions for the data recorded into the three different seismogram components, vertical, radial and tangential. I is the impulse response from the instrument, S is the source function and E is the impulse response from local Earth structure. The three functions I, S and E are convolved to form the seismogram, D.

Assuming that the $E_V(t)$ function from equation (1) is a Dirac delta function, equation (1) can be written as:

$$D_V(t) = I(t) * S(t) \quad (4)$$

Using this assumption, deconvolution of Fourier transform of horizontal seismograms (radial and tangential) data by the vertical seismogram data gives the receiver function in frequency domain (equation (5)).

$$E_R(\omega) = \frac{D_R(\omega)\overline{D}_V(\omega)}{D_V(\omega)\overline{D}_V(\omega)} G(\omega) \quad (5)$$

In equation (5), $\overline{D}_V(\omega)$ represents the complex conjugate of the Fourier transform of the vertical seismogram data $D_V(\omega)$ and $G(\omega)$ is a low-pass Gaussian filter applied to the receiver function to filter out high frequency noise where

$$G(\omega) = e^{\frac{-\omega^2}{4a^2}} \tag{6}$$

In the equation (6), a represents the Gaussian filter width parameter. The parameter dictates the boundary of the filtered frequency. In general, the filter gain for the Gaussian filter is 0.1 at ω = a/2. This means that the amplitude in the frequency domain is less than 10% of pre-filtered state if the frequency is higher than a/2. Because the Gaussian filter width parameter of 2.5 is widely used in receiver-function analyses, I used 2.5 for the parameter value in this research (Langston, 1977; Owens, 1984; Ligorria and Ammon, 1999).

In addition to applying a Gaussian filter, I calculated a fit between my receiver function results and results generated by receiver function iterative deconvolution method. The receiver function iterative deconvolution method uses a least squares minimization of the difference between the observed radial seismogram (equation 2) and signal estimated by convoluting vertical seismogram (equation 4) with an iteratively updated spike train. An initial estimate for this spike train is calculated by cross-correlation of the vertical and radial seismograms. The initial spike train convolutes with the vertical seismogram to find a misfit between the radial seismogram. Once this misfit becomes insignificantly small after many iterations, iteration stops and the resulting updated spike train obtained from this method becomes a receiver function result. I compared two deconvolution method results for the same event data in every station. If the fit is less than 80%, the receiver function is considered poor and will not be used to perform later steps. This criterion removes poor data that may introduce errors in my final results (Ligorria and Ammon, 1999).

After these data filtering and selection steps, the receiver function $E_R(\omega)$ is transformed into a time domain receiver function $E_R(t)$ using an inverse Fourier transform. $E_R(t)$ contains information on the local earth structure including timing and amplitude of seismic waves propagating through the structure beneath the receiver (Ammon, 2006) .

The radial receiver function is mainly used with teleseismic waves to determine the depth to the Moho layer below seismic stations. At teleseismic distances P waves approach seismic stations at a near vertical angle (Figure 7). When the waves reach the Moho, the boundary between the crust and upper mantle, the large velocity contrast causes some of the seismic P wave energy to convert to SV (or vertical S) wave energy. When this wave train approaches seismic stations, the approaching S converted P wave is called P_S. Since direct P and P_S waves travel in the crust at different velocities, the receiver function can give us information on the difference in arrival times for P and P_S. Using this time difference, the body wave velocities, ray parameter, and thickness of the crust can be calculated with equation (7).

$$H = \frac{t_{P_S}}{\sqrt{\frac{1}{V_S^2} - \rho^2} - \sqrt{\frac{1}{V_P^2} - \rho^2}} \tag{7}$$

Where t_{P_S} is the arrival time difference between P and P_S, V_S and V_P are S and P wave velocities, ρ represents ray parameter of incident wave, and H is the thickness in km (Zhu and Kanamori, 2000).

In the equation (7), the thickness is highly dependent on the velocity ratio V_P/V_S or κ. Therefore, to have an accurate thickness, the velocity ratio has to be very accurately determined. To better approximate κ, different seismic wave arrival times are used. After the P_S wave arrival,

there are teleseismic waves that reach the seismic station by making multiple reflections between the surface and the Moho. These waves are termed $P_P P_S$, $P_P S_S$ and $P_S P_S$ (Figure 4). Applying the arrival time difference between the direct P wave and these waves to equation (7) will narrow possible ranges of κ values and better determine the thickness value (Zhu and Kanamori, 2000).

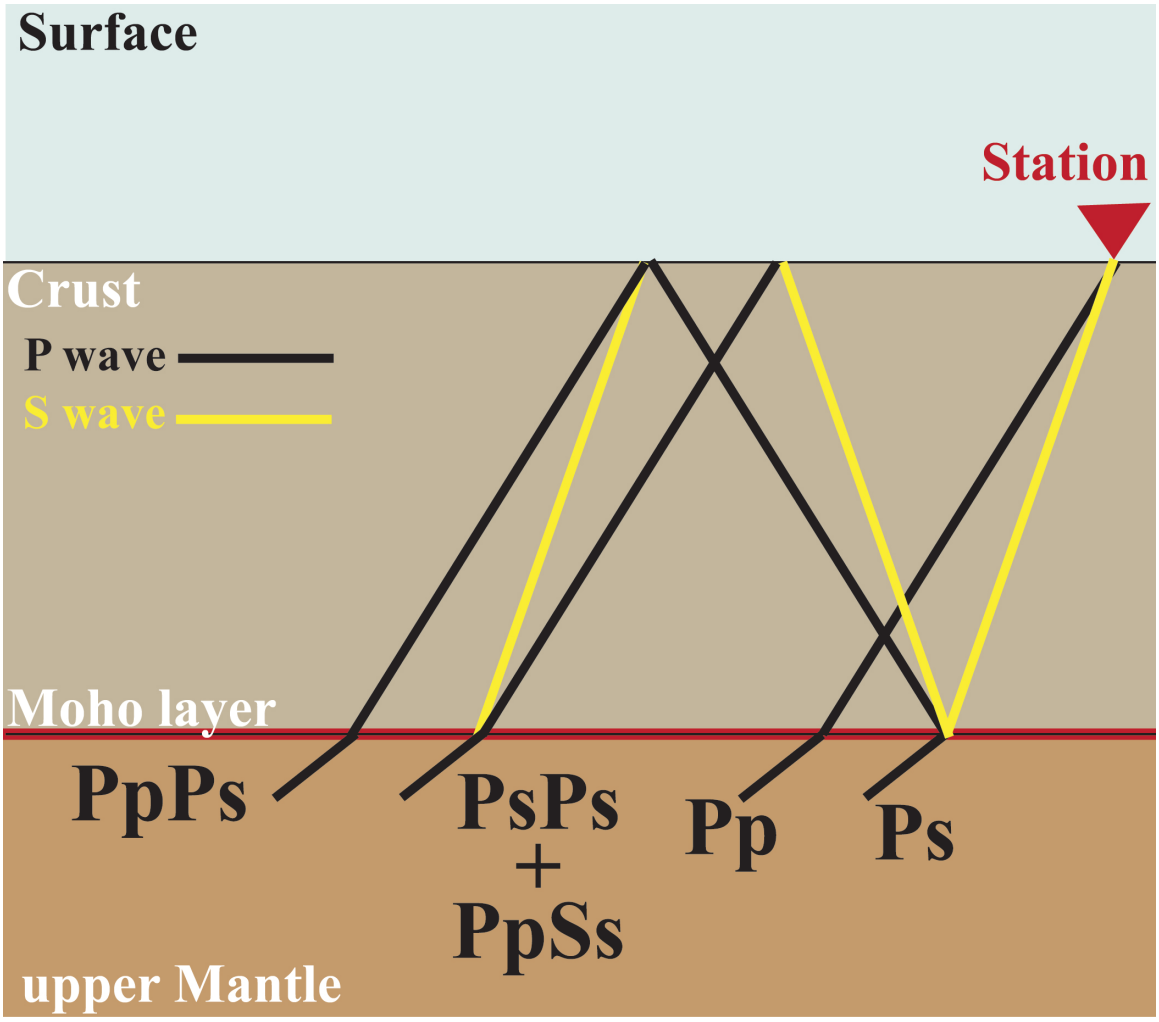

Figure 7: Types of teleseismic waves: The teleseismic P wave interacts with the crust/mantle boundary (Moho) to form different types of seismic waves. In this figure, P waves (black lines) and S waves (yellow lines) travel from the left to the right toward the receiver station (triangle). These waves convert from P to S or S to P when they reach the surface or the Moho (Zhu and Kanamori, 2000).

Stacking

With ideal receiver function data, the above method can give us enough information to find the depth and κ. However, with real receiver function data, noise will cause miscalculations. Therefore, the deconvolution process works best when the signal to noise ratio of the data is high. This means that receiver function approach gives us better results with data from large seismic events and data with less noise (Ligorria and Ammon, 1999).

To improve receiver function results, Zhu and Kanamori (2000) created stacking methods that allow us to stack multiple earthquake data at a station. The stacking equation is:

$$S(H,\kappa) = \omega_1 r(t_1) + \omega_2 r(t_2) - \omega_3 r(t_3) \qquad (8)$$

In (8), function r(t) represents the radial receiver function at the arrival time of three different waves (P_S, $P_P P_S$ and $P_P S_S + P_S P_S$), and the ω are weighting factors where $\sum \omega_i = 1$. In my research I used a factor ratio of 0.3+0.5+0.2, 0.4+0.3+0.3 and 0.5+0.4+0.1. S is a function of the Moho depth and κ and the sum of this function S for every earthquake can be plotted into 3D plot (Figure 8). This plot shows the variation of receiver functions and indicates the most probable H and κ at Maximum S(H, κ) . For this method, increasing the number of receiver function data for a station provides better and more stable H and κ values. However, at the same time, if there is any receiver function data that are corrupted, the corrupted data produce errors to the maximum S(H,κ) value. In order to mitigate errors to my results, these erroneous data must be removed manually from the stacked results (Zhu and Kanamori, 2000).

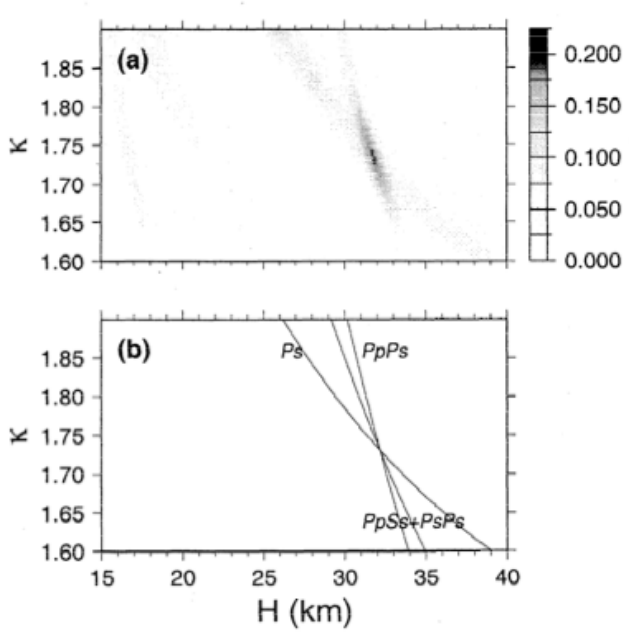

Figure 8: Illustration of how equation 6 can be plotted in 3D. The X axis represents Moho depth, Y axis represents velocity ratio, κ and color (Z axis) on (a) represents S(H, κ). S(H, κ) reaches a maximum at the point where the slopes of different body waves intersect (b). By stacking multiple events, the maximum of S(H, κ) indicates the most likely values of H and κ (Zhu, and Kanamori 2000).

Kriging

Once receiver functions are calculated, 3D maps are generated based on locations of receiver stations (longitudes and latitudes) and receiver function values (Vp/Vs and H). However, since the receiver function only calculates values at receiver stations, there are no receiver function values in areas between receiver stations. In order to determine receiver function values at unobserved areas, I am applying a spatial interpolation method called Kriging.

Kriging assumes that the spatial variation of data (in my case, the velocity ratio and crust thickness) is neither random nor deterministic. Rather it assumes that the variation is composed of 3 different components. The first component is the variation caused by regionalized / spatial influence. The second component examines the variation caused by structure and the third component represents variation caused by random errors (Chang 2008). In my project, I used one type of kriging called Ordinary Kriging. This Kriging only examines the first component, the specially correlated component, to fill in unknown data values at unobserved locations.

Variograms And Semivariance

Kriging is an application of geostatistics. Based on the statistics of data with spatial information, it generates data for area with no data. Therefore, to apply kriging to our data, I need to statistically analyze my data values (Vp/Vs and H) with variograms (Trauth 2007).

The term "semivariance" is used to express the spatial dependence of data. This semivariance is computed by using equation (9)

$$\Gamma(h) = \frac{1}{2}\left[z(x_i) - z(x_{i+h})\right]^2 \qquad (9)$$

In this equation, Γ represents the semivariance between two points x_i and x_{i+h} that are separated by the distance of H. z represents the data values at these two points. By continuously calculating semivariance for 2 different points in my dataset, I create a variogram cloud. A variogram cloud plots Γ against the distance between two data points (lag size) and shows the range of semivariance values at different distances (Chang 2008).

The variogram cloud is an important for analyze the spatial dependency of the data. However, it is hard to make use of a variogram cloud with many semivariance data points at different distances. To solve this problem, I applied a process called binning. The process of binning reorganizes variogram points by distances and directions. It then computes average semivariance by different distances. In a binning process, lag sizes are separated into groups called lag classes. So for instance, in my process of reorganization, any pair of data points within a lag size of less than 2000 meters belongs to the lag class of 0-2000 and lag size between 2000 and 4000 meters are separated into a different lag class of 2000-4000. Moreover, the binning also groups pairs of data points by direction. After distributing pairs of data points by distance and direction, binning calculates the average semivariance for semivariance values at the same lag size (Chang 2008).

$$\Gamma(h) = \frac{1}{2n}\sum_{i=1}^{n}[z(x_i) - z(x_{i+h})]^2 \qquad (10)$$

Equation (10) is used to compute the average semivariance. Γ as a function of H is the average semicariance, n is the number of pairs of data points (x_i and x_{i+h}) found in the same lag size (H) and z is the data value at x_i and x_{i+h} locations.

After applying the binning process to my data, the new variogram plot shows the average semivariances at certain range of lag size (lag group). The new plot helps me create a

semivariance model for the kriging process. If sufficient amount of data are available, the plot also allows me to compare semivariances values averaged over different directions.

Models For Kriging

Once an average semivariogram is computed, a mathematical model that fits with the average semivariogram replaces the average semivariogram values since the ordinary kriging method requires semivariance values between a known point and an estimated (unobserved) point. Since my average semivariogram only contains semivariance values at the distance between 2 known points, it is discrete. In order to find the semivariance between known and estimated points, I need to construct a continuous plot that contains semivariance values at every distance (Trauth, 2007).

Ordinary Kriging

The ordinary kriging method was used to estimate the velocity ratio and crustal thickness of an unobserved point. The equation for these estimated values is:

$$\hat{Z}_0 = \sum_i^N W_i \cdot Z_i \tag{11}$$

where $\hat{Z}_0$ is the estimated value at a location where there is no seismograph station, N is the number of sample points used in the estimation, Z is the known value at point i and W is the weight associated with point i (equation 12).

$$\sum_i^N W_i = 1 \tag{12}$$

Therefore, the estimated value can be calculated only if the weights for data points are known.

The values for weights are calculated using following equation.

$$\gamma(x_i,x_0) = \sum_{j=1}^{S} W_j \gamma(x_i,x_j) + \lambda \tag{13}$$

where $\gamma(x_i,x_0)$ is the semivariance between the data point *i* and unobserved point, $\gamma(x_i,x_j)$ is the semivariance between 2 known data points *i* and *j*, *S* is the number of sampling points and λ is a Lagrange multiplier added to ensure the minimum estimation error. Since values for $\gamma(x_i,x_0)$ and $\gamma(x_i,x_j)$ are known from the model, use of equations 12 and 13 makes an overdertermined system where the weighting factors are the only unknowns.

For example, assuming there are 3 sampling points, equations that are used to solve weights are:

$$\begin{aligned}
&W_1\gamma(x_1,x_1) + W_2\gamma(x_1,x_2) + W_3\gamma(x_1,x_3) + \lambda = \gamma(x_1,x_0)\\
&W_1\gamma(x_2,x_1) + W_2\gamma(x_2,x_2) + W_3\gamma(x_2,x_3) + \lambda = \gamma(x_2,x_0)\\
&W_1\gamma(x_3,x_1) + W_2\gamma(x_3,x_2) + W_3\gamma(x_3,x_3) + \lambda = \gamma(x_3,x_0)\\
&W_1 + W_2 + W_3 + 0 = 1
\end{aligned}$$

Once weights are calculated by solving an overdetermined system, the estimated value for the unobserved point, $\hat{Z}_0$, can be calculated using equation 10(Trauth 2007; Chang 2008).

RESULTS

Before generating receiver function results, we checked numbers and locations of receiver stations with event data in Texas. Figure 9 shows stations with event data in red. With this map, there are several areas with no data. The reason why there are no data in some regions is because SOD does not process event data for stations that do not have correct azimuth for North and East. When station collects seismic data from a 3-component seismogram, horizontal seismograms are set in 2 directions North-South and East-West. The SOD program does not process events data from stations if these horizontal seismograms are not placed correctly.

In order to gain data from these unprocessed stations with SOD, we adjusted header files of stations and corrected azimuth. The figure 10 shows the stations with event data after I made this adjustment. With this adjustments, numbers of event data increased from 0 to 10~20 event data.

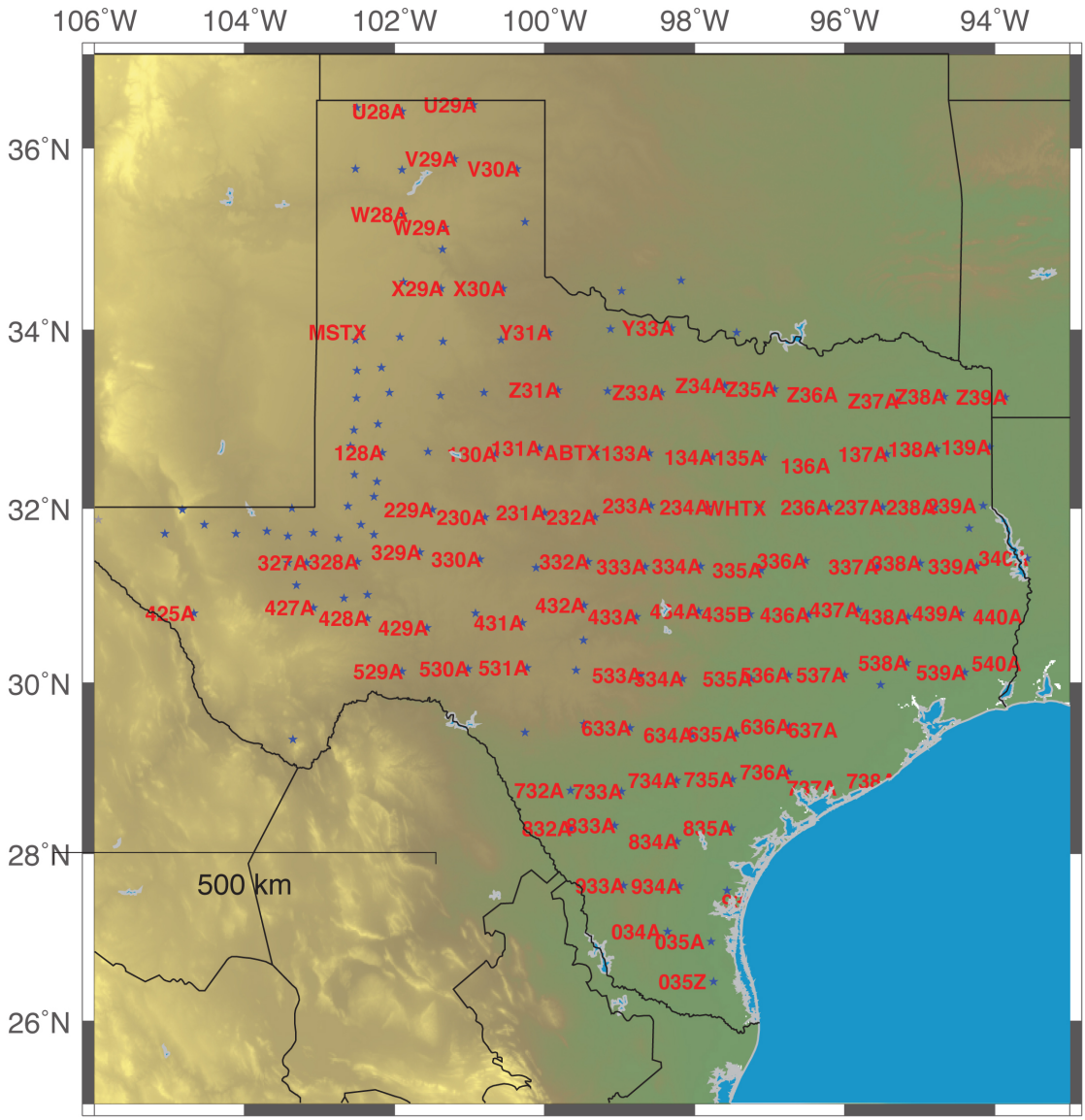

Figure 9: Locations of receiver stations in Texas before azimuth adjustment

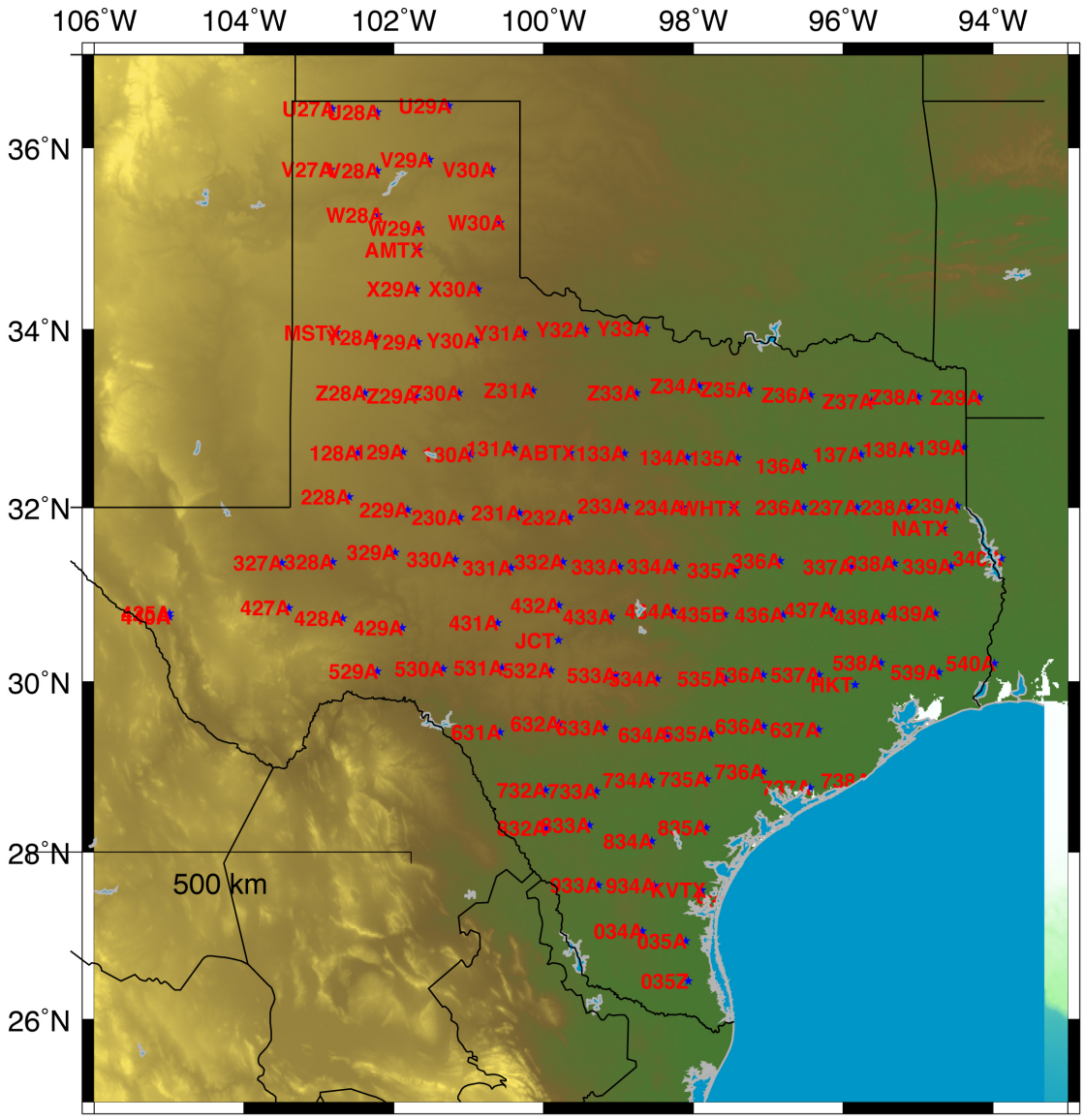

Figure 10: Locations of receiver stations in Texas after azimuth adjustment

Initial receiver function results were calculated using 4-3-3 weighting for stacking and an exponential model for kriging (figure 11 and 12). For crustal thickness, the 3D plot shows a thicker crust in central and Northwestern Texas compare to the coastal region in east Texas. However there is a region in central Texas where thickness is lower than 35km. Our seismic velocity results shows unusually small ratio values for the area where crustal thickness is shallow (around 35km). Only exception for this observation is Permian basin area in west Texas. In this area, the thickness range from 37.5 to 45km and the velocity ratio ranging from 1.6 to 1.7.

To verify the rationalities of these receiver function stacking results, I generated a GMT map of Texas showing numbers of event data that were used to create receiver function stacking results (Figure 13). The figure 13 tells us that there are significantly small amount of data used to perform receiver function stacking for eastern Texas. Because deployments of USArray stations in east Texas started late 2010, stations in east Texas have less event data to calculate receiver function than rests of USArray stations in Texas. The receiver function results generated from few event data are less credible than one with more data. Since the stacking method works better when various event data are overlaid on a stacking window, receiver function results from stations with small amount of data may produce wrong crustal thickness and seismic velocity ratio values (figure 14). Thus, for our receiver function results I do not have enough data to compute correct receiver function results for east Texas.

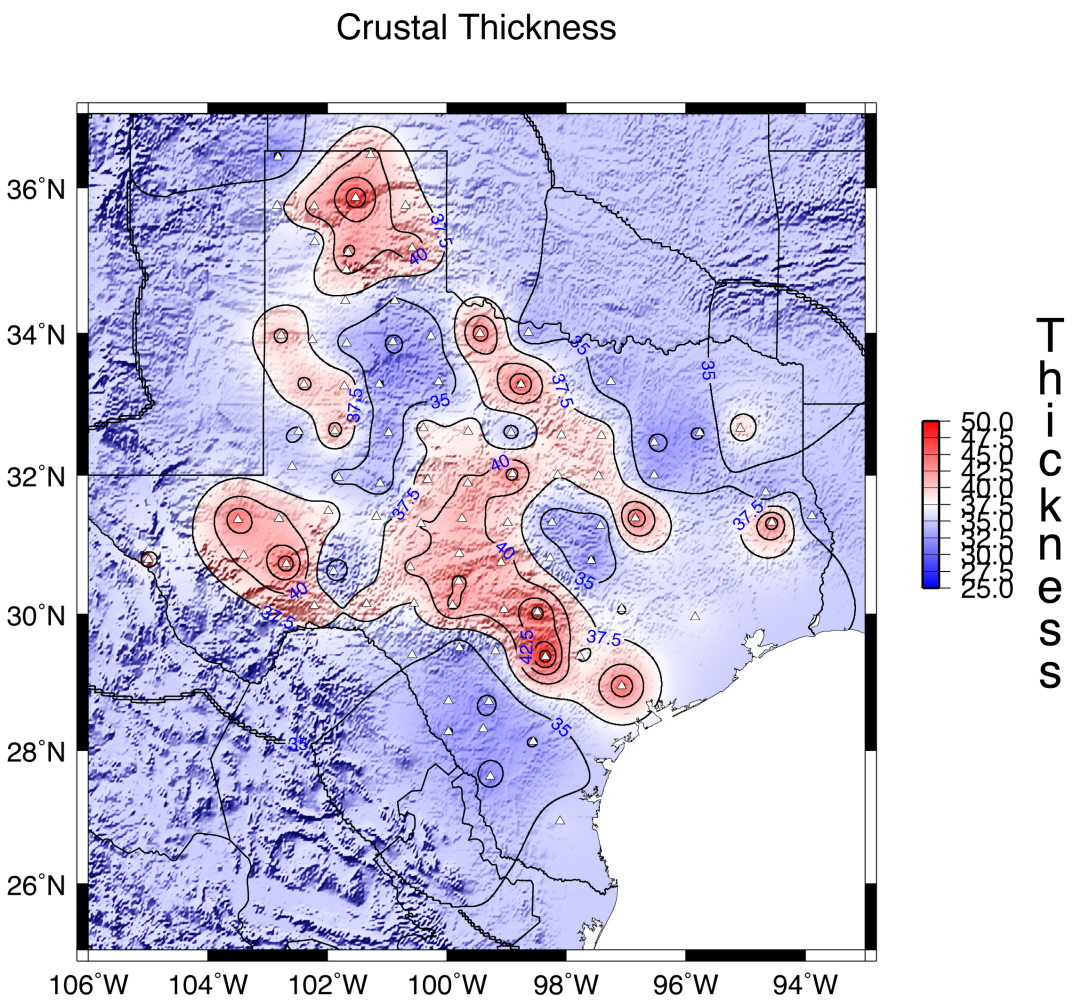

Figure 11: Initial receiver function result for crustal thickness in Texas

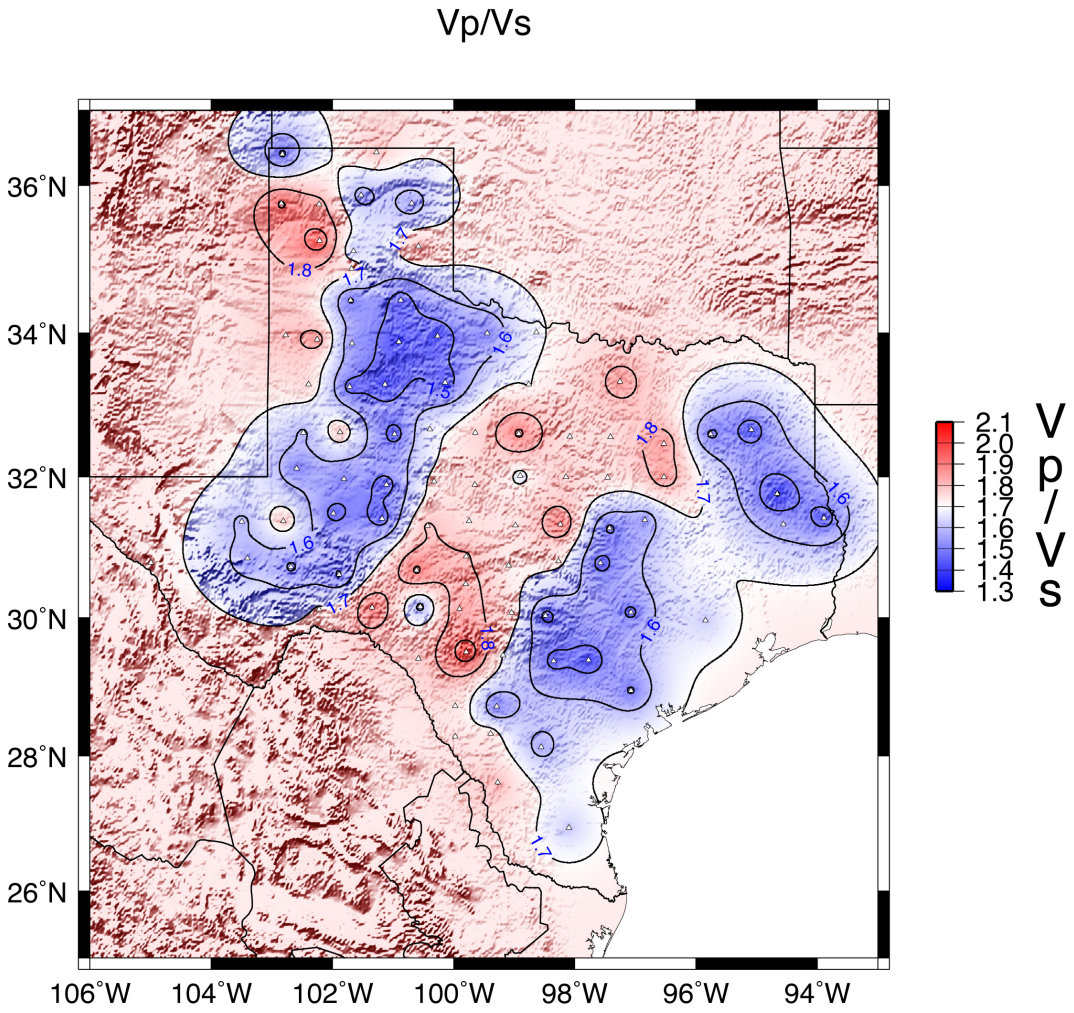

Figure 12: Initial receiver function result for velocity ratio in Texas

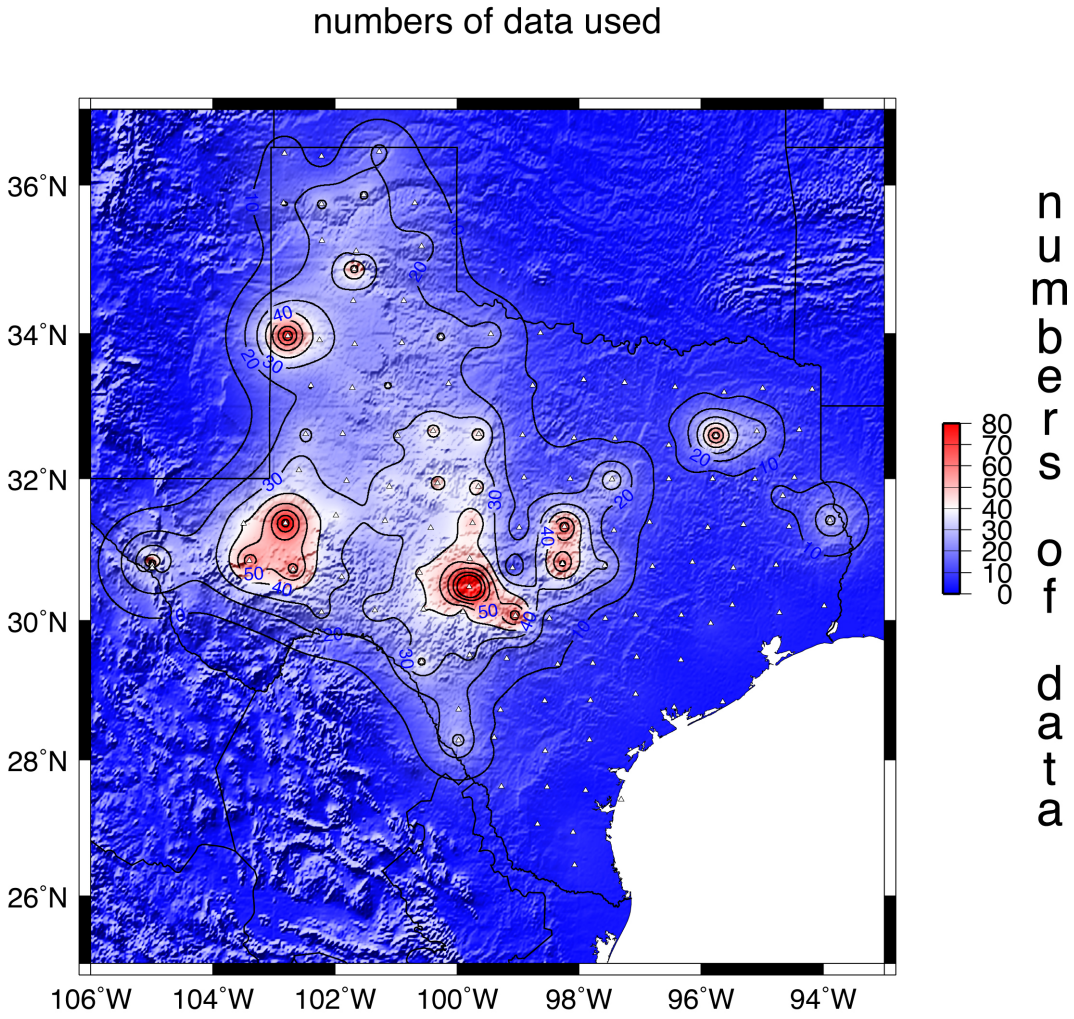

Figure 13: 3D plots of the number of event data used in receiver stations in Texas: due to the deployment dates for coastal region seismic stations, I did not have enough data to obtain receiver function stacking results for East Texas. However I was able to get good amount of data for central and west Texas, particularly for the Reference Network stations.

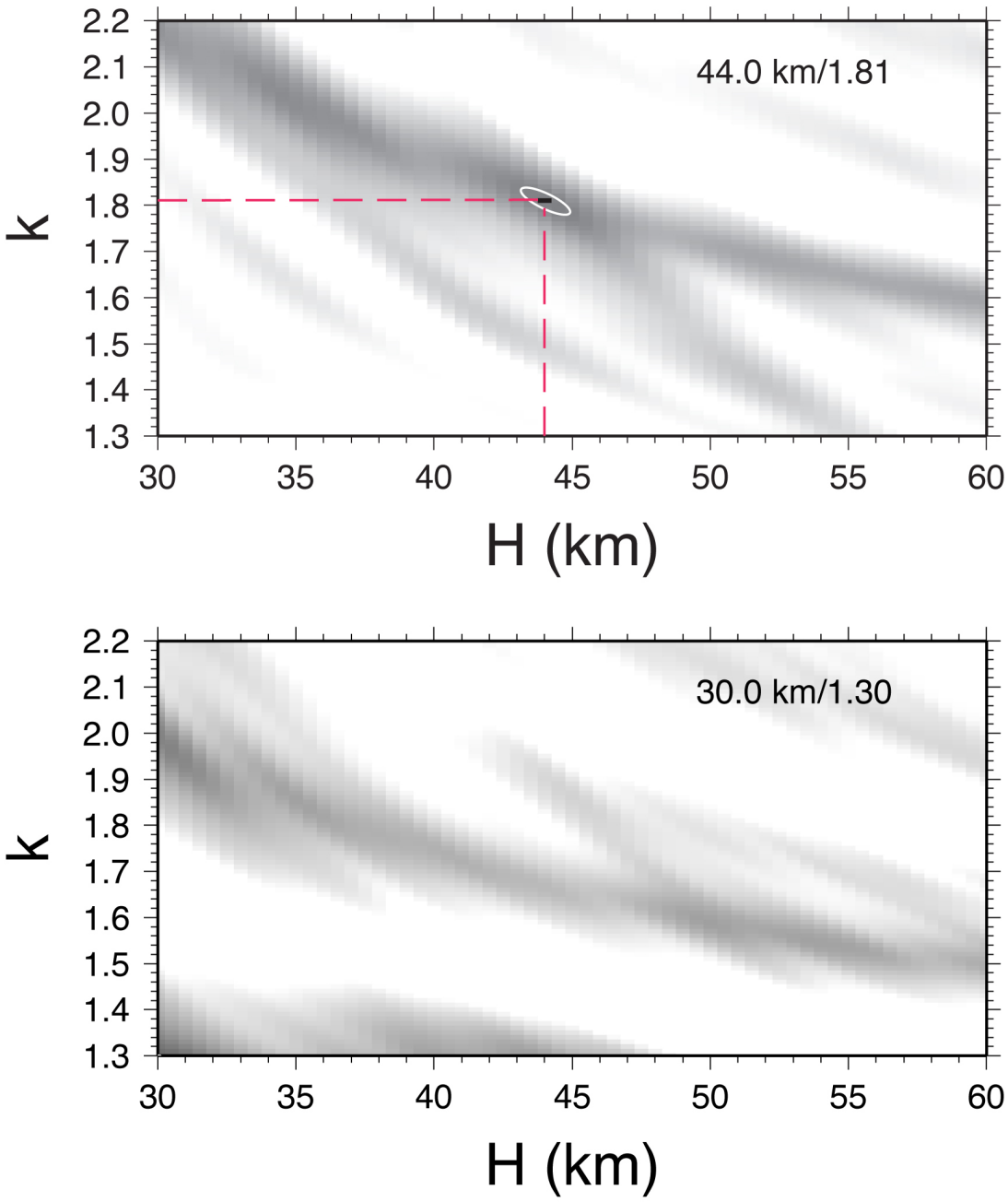

Figure 14: Results of stacking method: the stacking result from station MSTX (above) and 733A (bottom). The result from MSTX shows an ideal result of the stacking method at reasonable depth and velocity ratio. The result from station 733A did not stack well and shows S (H, κ) at the minimum boundary. This means that at 733A, there are data that are possibly corrupted or the station had small amount of event data used for the stacking method. With MSTX, I had 81 event data and with 733A I only had 6 event data available to perform stacking.

DISCUSSIONS

The receiver function results from Rio Grande rift in East New Mexico and West Texas are shown on Figure 15 and 16. In Figure 15, the Rio Grande rift is characterized by thin crustal thickness zone (30-35km) surrounded by thicker mountain ranges (37-42km) in New Mexico. Based on this observation, location of Rio Grande rift is estimated (Figure 15).

Unlike crustal thickness, the velocity ratio of Rio Grande rift (Figure 16) does not show velocity ratio values that characterize rift system. Since high velocity ratio means slower shear wave velocity and shear waves travel slower in molten structure, the high velocity ratio value usually indicates the existence of heat source under receiver station. Although velocity ratio value in New Mexico and west Texas on Figure 16 shows wide variety in the range, rift zone estimated by crustal thickness has velocity ratio value of 1.7-1.8, a typical velocity ratio value for crusts (Thompson 2011).

Sosa A., 2011, generated a cross section map for this area using joint inversion method between receiver function from Thompson and surface wave data (figure 17). The line of cross section overlaps the boundary between Texas and New Mexico where large velocity ratio change was observed in receiver function results (Figure 16). According to his figure, area west of estimated Rio Grande rift at 32 degrees North has crust that is composed of two different shear wave velocity structures. In the area, there is one velocity contrast within crust at 30km depth and this contrast separates upper crusts where shear wave travels slower and lower crust s where shear wave travels faster. Between high velocity ratio area and low velocity ratio area, range of shear wave velocity seems to be similar for most of the depth except for the upper crusts. The mid-crust velocity contrast shown in this figure can influence receiver function results significantly. Receiver function uses reflection and change of seismic waves at velocity contrast

at the Moho and captures depth of the Moho. If velocity contrast exists within crust, receiver function could capture the depth of this velocity contrast instead of one at the Moho.

Applying this observation of mid-crust velocity contrast, we revisit our initial receiver function result and made a small change in the stacking processes. Since I was doubtful about several receiver stations in central Texas (figure 18) showing low crustal thickness, we assume that the resulting thin thickness for these stations reflects a mid-crust velocity contrast and not the Moho. In order to capture the Moho depth, we adjusted the window size of stacking window from 30km to 60km depth range to 37km to 70km depth range (Figure 19).

The receiver function results after the change is illustrated on Figure 20 and 21. After this change in window size, the thin crust area in central Texas disappeared and crusts become much thicker in the area. The change in window size did not influence new velocity ratio results. Many areas still show significantly low value for velocity ratio especially at the corner of New Mexico and Texas boarder. This result may be indicating that low velocity ratio is caused by some unknown geological properties that help S wave propagate faster or failure of stacking. Since this low velocity ratio area near the state boarder is on the Delaware Basin, in the future study, more detailed investigations on the receiver function results of this area should be performed by making comparisons with other geophysical study done in this area such as well logging data. Since well log data usually contains structural, density and velocity information of the crust, use of well logging data can help us understand the reason why some areas have low velocity ratio for their receiver function results.

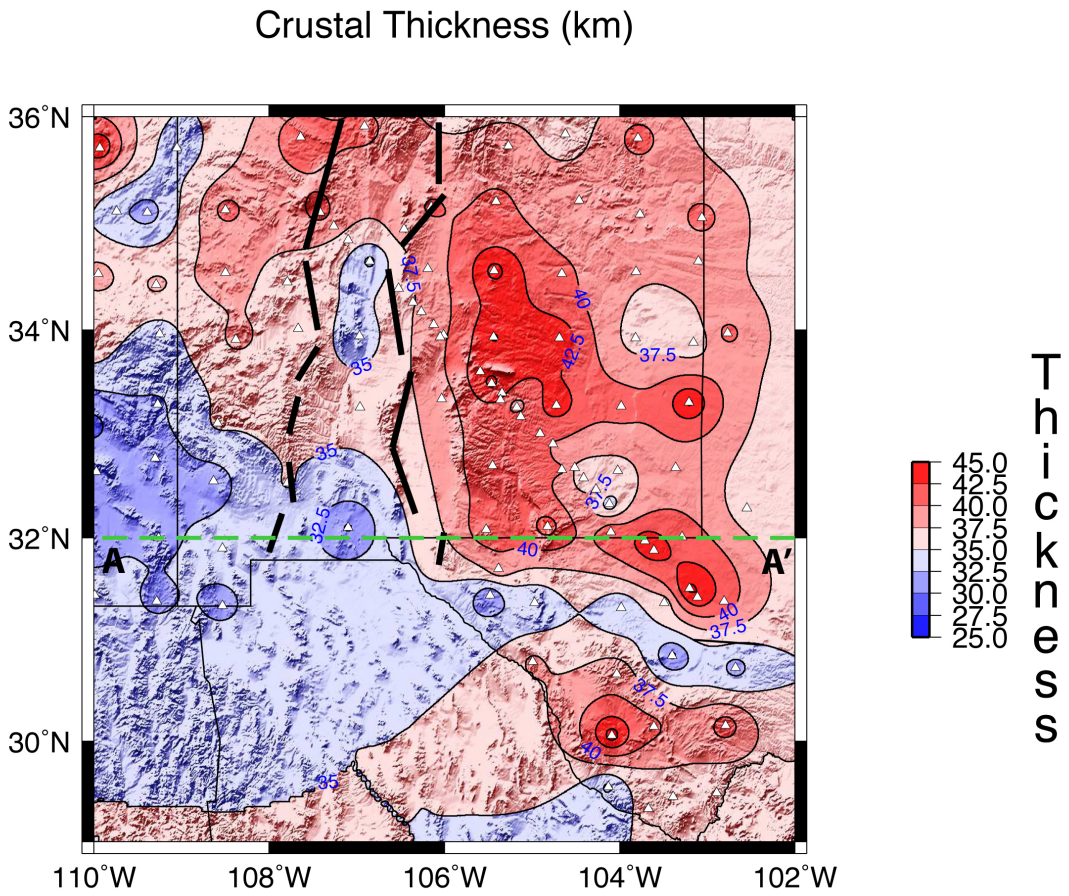

Figure 15: Receiver function results of Rio Grande rift zone (crustal thickness): The area surrounded by black dashed line represents estimated area of the Rio Grande rift zone. This area is composed of thin crustal area surrounded by thick mountain range. The green dashed line is the line covered by the cross section map (Figure 17) (Thompson 2011).

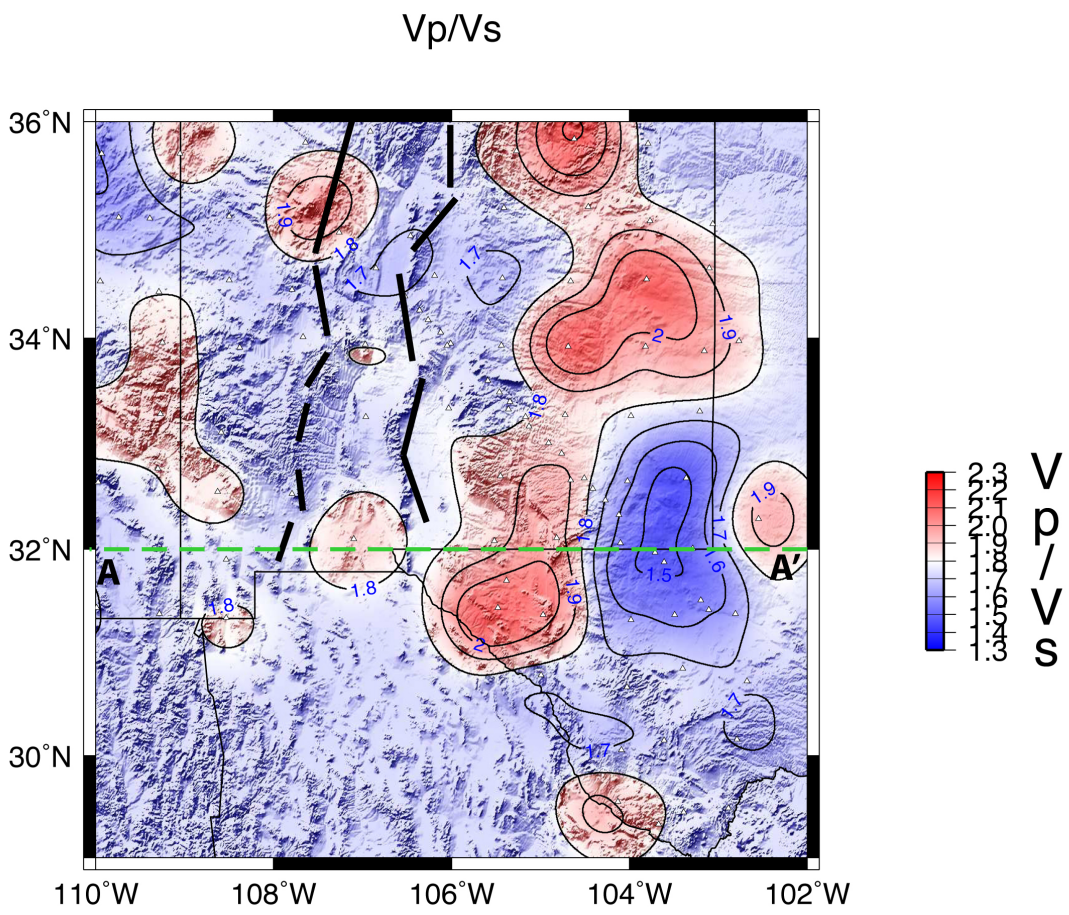

Figure 16: Receiver function results of Rio Grande rift zone (velocity ratio): Black dashed line surrounds Rio Grande rift zone estimated from crustal thickness (Figure 15). Unlike Figure 15, the estimated area does not have any range or characteristics of velocity ratio that separates this estimated area from other. The green dashed line is the line covered by the shear velocity cross section map (Figure 17) (Thompson 2011).

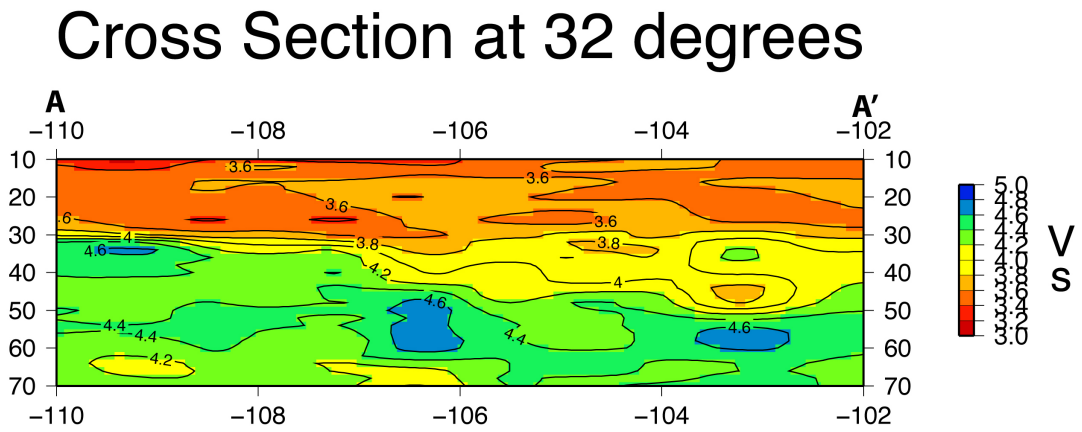

Figure 17: Shear wave velocity cross section map generated with joint inversion method by Sosa A. , 2011. This map represents the green dashed line on Figure 15 and 16. Using joint inversion method, this map shows an existence of mid-crustal velocity contrast within crusts.

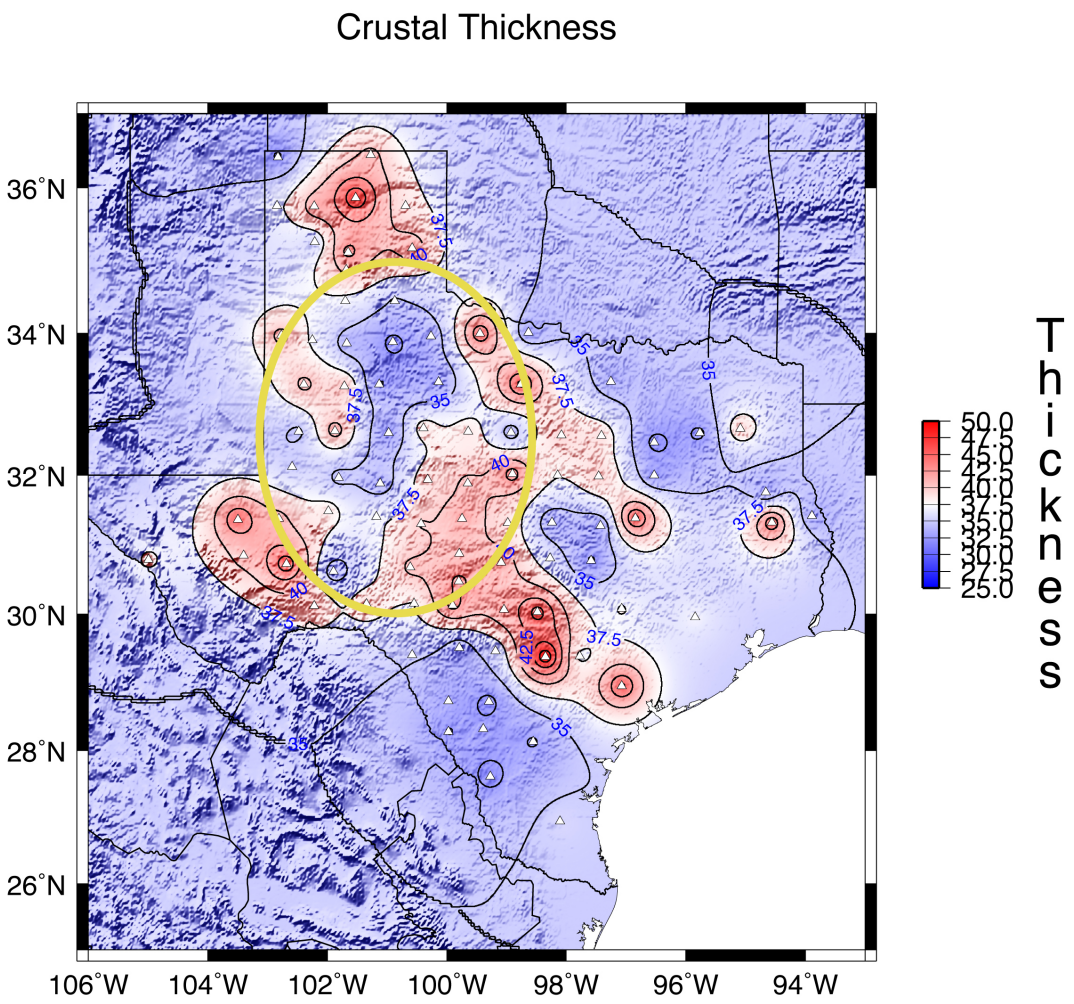

Figure 18: Initial crustal thickness estimation in central Texas (area with in yellow circle) may reflects mid-crust velocity contrast and not the Moho velocity contrast.

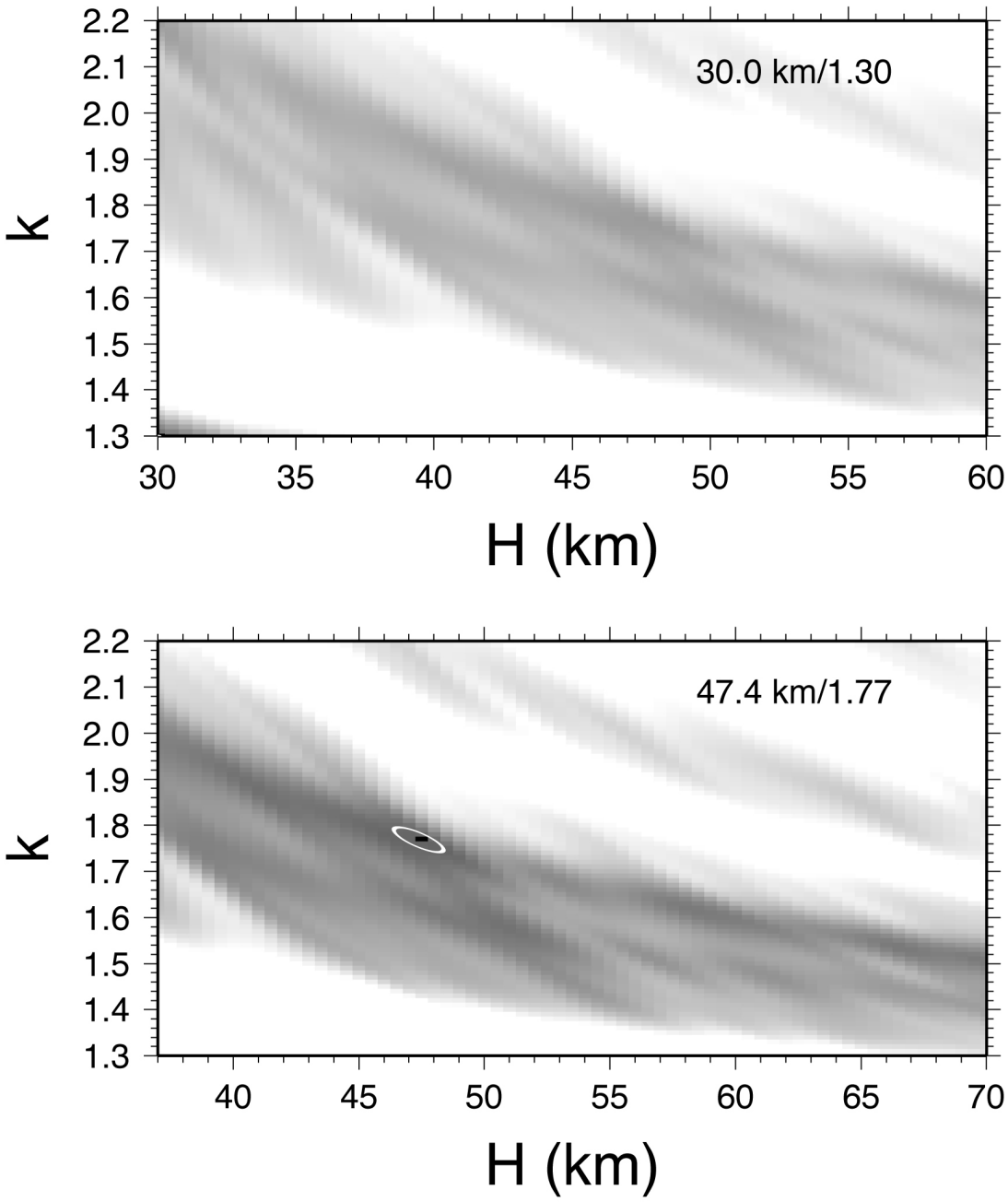

Figure 19: Results of stacking station Z30A: before changing window size of stacking method (30 to 60kn for depth) (up) and after changing window size of stacking to 37 to 70km (bottom).

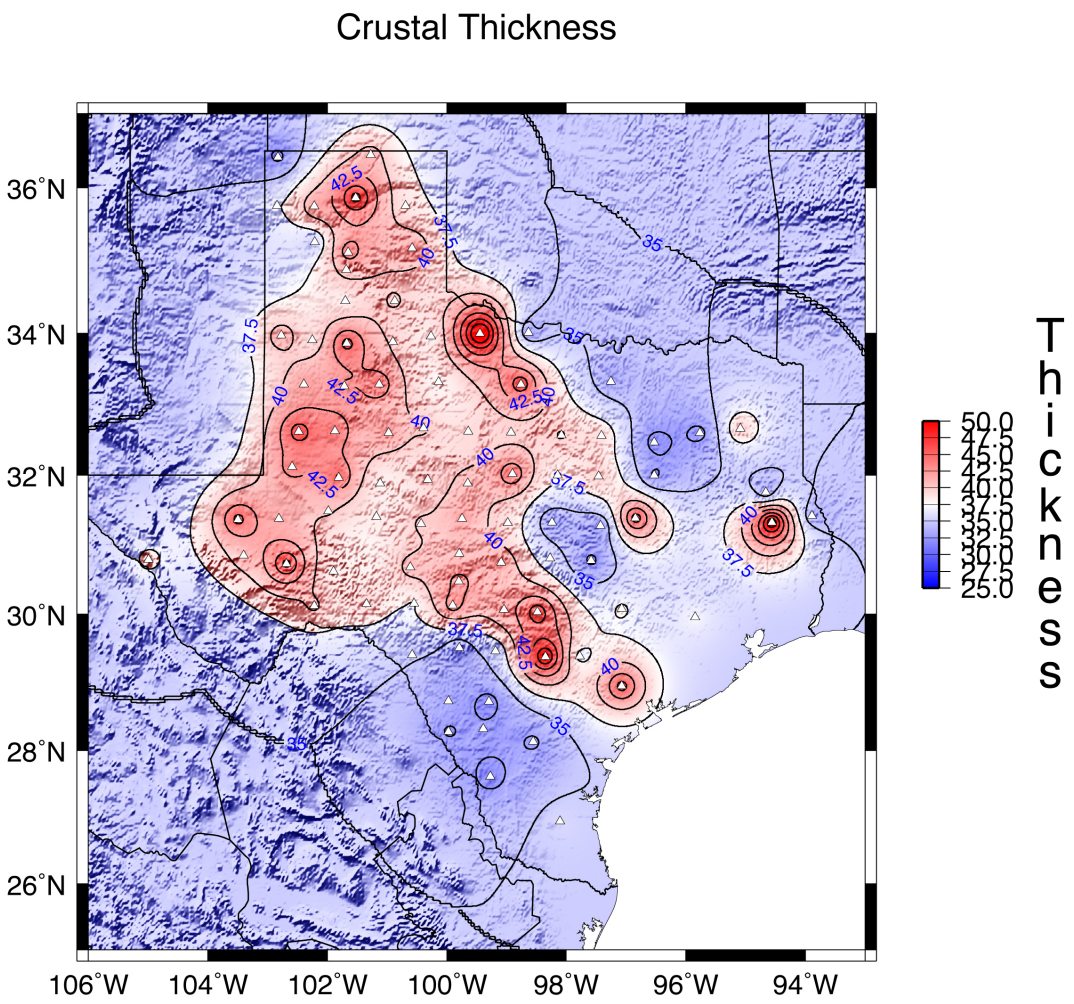

Figure 20: Receiver function thickness result after changing window size of stacking window

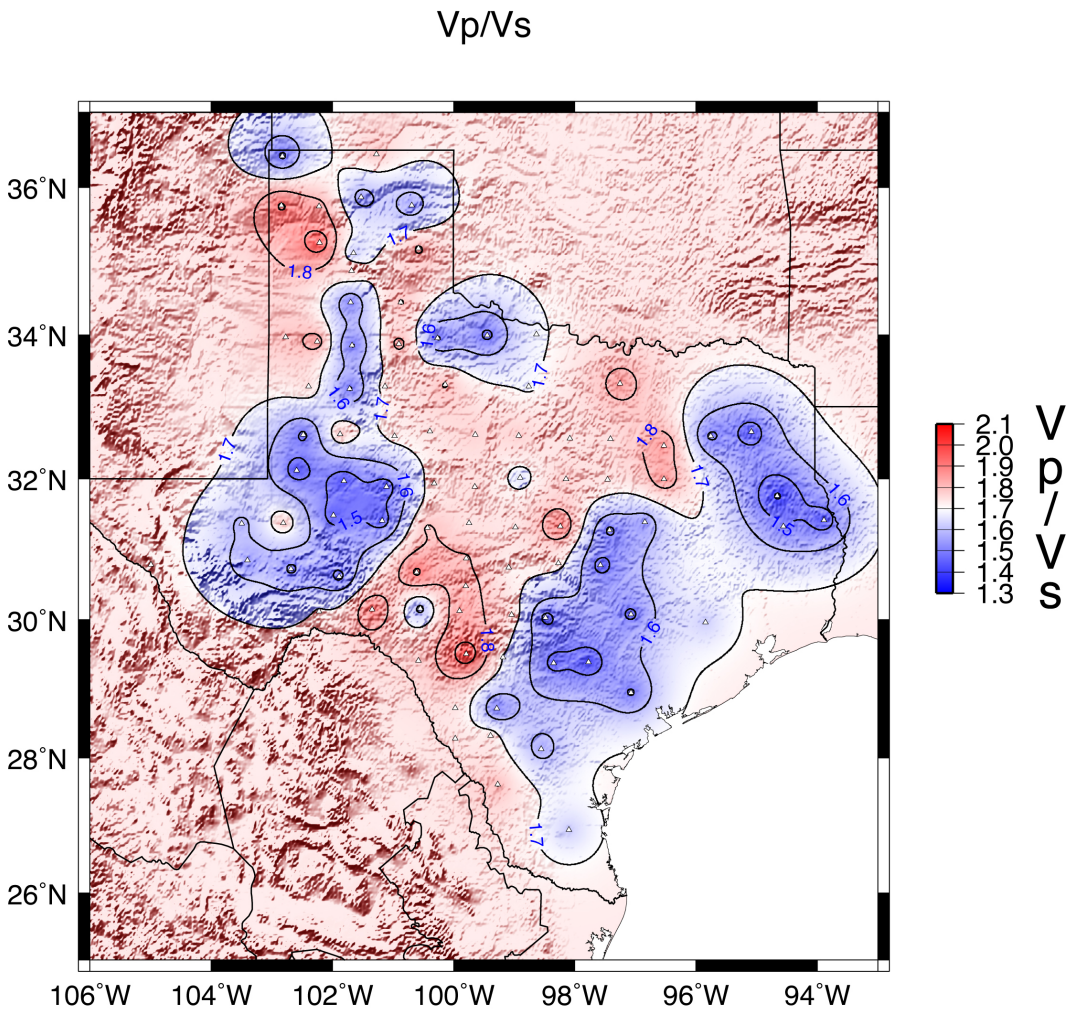

Figure 21: Receiver function velocity ratio result after changing window size of stacking window

Figure 22 and Figure 23 is my improved receiver function results with geological provinces overlaid. My results show that thickness tends to increase toward northwestern direction. Although we cannot say that coastal region has good thickness results, the direction of crustal thickness increase in my results correspond to the direction of age increase on my Texas geological provinces map. Also there are two stations on the boarder of Mesoproterozoic Craton and Transitional Crust showing thick crustal thickness. We don't have too much data for these two stations however, these results maybe reflecting the Ouachita orogen which formed during Pangea formation in the Pennsylvanian time. We also see low and high velocity ratio values

along South Oklahoma Aulacogen. Since in South Oklahoma Aulacogen areas, we find mafic bodies and high dense materials, adding some Oklahoma and New Mexico stations to the lists of seismic stations may help understanding mafic bodies' influence on velocity ratio.

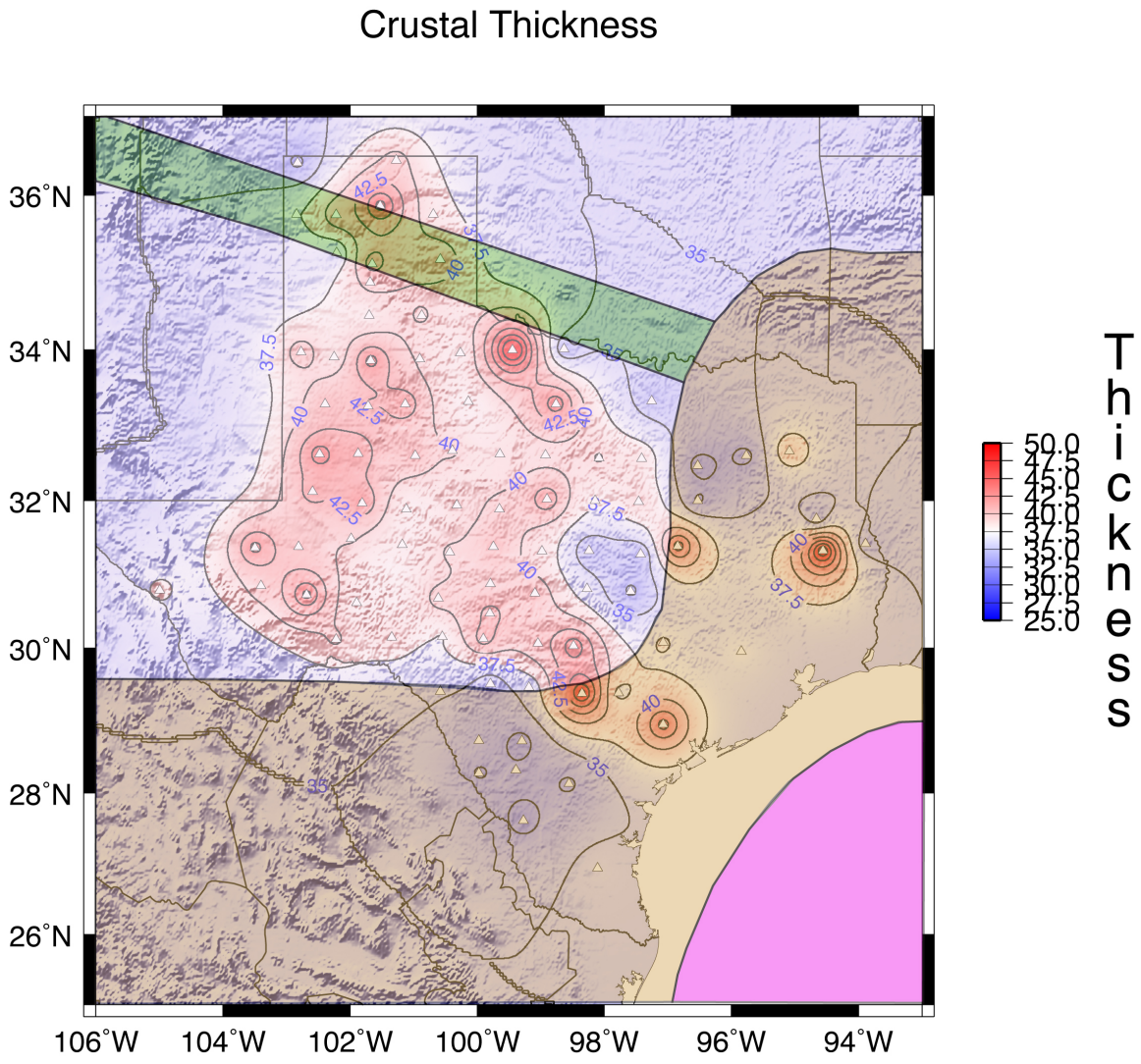

Figure 22: Improved receiver function crustal thickness result with geological provinces of Texas.

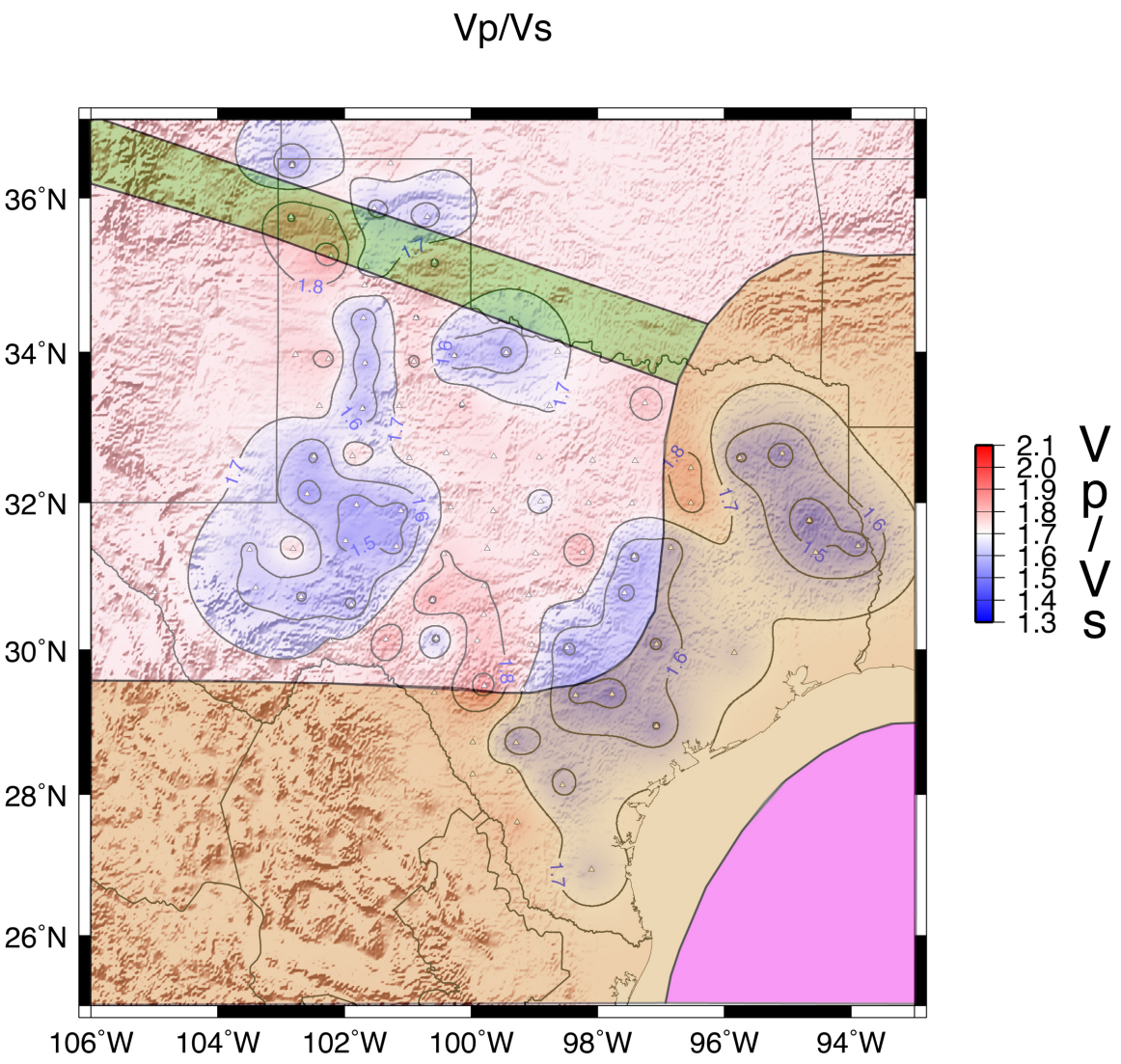

Figure 23: Improved receiver function receiver function result with geological provinces of Texas.

CONCLUSION

Although good connections between the receiver function results from Rio Grande and from Texas are hard to make, from this comparison, we found that Rio Grande rift has much shallower crustal thickness than Texas. From Rio Grande result, we see that active rift zones have a thickness < 35km. Moreover, both results show similar results for the velocity ratio in West Texas. Some crustal rock components might be influencing seismic velocity at the low ratio region. Further data collection for coastal area and application of joint inversion method with surface wave data will probably enhance the understanding of velocity structures and crustal depth of Texas.

References

[Adams, D.C. and Keller, G.R, 1993, Possible extension of the Midcontinent Rift in west Texas and eastern New Mexico, *Canadian Journal of Earth Sciences,* 31, 709-721.]

[Ammon, C. J. 2006. Receiver-Function Analysis, Pennsylvania State University, Web page: http://eqseis.geosc.psu.edu/~cammon/HTML/RftnDocs/rftn01.html]

[Anthony, E.Y., 2005, Source regions of granites and their links to tectonic environment: Examples from the western United States: *Lithos*, v. 80, p. 61–74]

[Corner, B., Cartwright, J., and Swart, R., 2002, Volcanic passive margin of Nambia: A potential fields perspective, in Menzies, M.A., *Vlocanic Rifted Margins: Geological Society of America Special Paper 362*, 203-220.]

[Chang, K., 2008, Kriging, *Introduction to Geographic Information Systems fourth edition*, 337-342.]

[IRIS, 2011, EarthScope Data, Web page: http://www.iris.edu/earthscope/usarray/]

[Langston, C. A., 1979, Structure under Mount Rainier, Washington, inferred from teleseismic body waves, *Journal of Geophysical Research,* Vol. 84, 4749-4762.]

[Ligorria J.P. and Ammon C.J., Iterative Deconvolution and Receiver-Function Estimation, *Bulletin of Seismological Soceity of America,* October 1999, 89,5,pp.1395-1400.]

[Mickus, K., Stern, R.J., Keller, G.R. and Anthony, E. Y., 2009, Potential field evidence for volcanic rifted margin along the Texas Gulf Coast, *Geology*, Vol 37, No. 5, 387-390.]

[Mosher, S., Levine, J.S.F. and Carlson, W.D., 2008, Mesoproterozoic plate tectonics: A collisional model for the Grenville-aged orogenic belt in the Llano uplift, central Texas, *Geology*, Vol 36, No. 1, 55-58.]

[Owen, T.J., 1984, Seismic Evidence for an Ancient Rift Beneath the Cumberland Plateau, Tennessee: A Detailed Analysis of Broadband Teleseismic P Waveforms, *Journal of Geophysical Research,* Vol. 89, No. B9, 7783-7795.]

[Raye U., Anthony E.Y., Stern R.J., Kimura J., Ren M.,Qing C. and Tani K., 2011, Composition of the mantle lithosphere beneath south-central Laurentia: Evidence from peridotite xenoliths, Knippa, Texas, *Geosphere*, June 2011; v. 7; no. 3; p. 1-14;]

[Sosa A., 2011, Joint Inversion for Crustal and Mantle Velocity Structure in the Southern Rio Grande Rift, presented in *American Geophysical Union Fall meeting 2011*, San Francisco CA.]

[Thomas W.A., 2006, Tectonic inheritance at a continental margin, *GSA Today,* v. 16, No 2. Feb. 2006]

[Thompson L.E., Velasco A.A. and Hussein M.,2011, Seismic Evidence for an Active Southern Rio Grande Rift, The University of Texas at El Paso, El Paso, TX.]

[Trauth M.H., 2007, Geostatistics and Kriging (by R. Gebbers) *MATLAB Recipes fir Earth Sciences Second Edition*, 206-224.]

[Zhu, L. and Kanamori, H., 2000, Moho depth variation in Southern California from teleseismic receiver functions. *Journal of Geophysical Research,* Vol. 105, NO. B2, 2962-2980.]

Curriculum Vita

Keisuke Irie was born in Tokyo, Japan, on December 5, 1986, the first and only child of Keita Irie and Kayo Irie. After graduating Ramapo high school in Franklin Lakes, NJ, He enrolled in Lehigh University, Bethlehem, PA as an environmental engineering major in September 2005. After spending 2 semesters at Lehigh University, in August 2006, he transferred to Cornell University, Ithaca, NY and changed his major to the Science of Earth System and studied geophysics. He graduated Cornell University with a Bachelor of Sciences degree in May 2009 and he worked as a research assistant for Dr. Larry Brown at Cornell University for half year after his graduation. His research on the ambient noise seismic interferometry was presented on AGU, American Geophysical Union, meeting in San Francisco, on December 2009. He was accepted into the Geophysics graduate program in 2010 at the University of Texas at El Paso and studied under Dr. Aaron Velasco. In the summer of 2011 from May to August Keisuke had an internship with Marathon Oil Corporation in Houston, Texas. He was offered a full-time position as a geophysicist with Marathon Oil Corporation. He graduated from the University of Texas at El Paso with his Master of Science degree in December 2011.

Permanent address: Matsugaoka 5-13-23, Kugenuma District
Fujisawa City, Kanagawa Prefecture, Japan

This thesis/dissertation was typed by Keisuke Irie